Spontaneous self-assembly of Perovskite nanocrystals into electronically coupled supercrystals : toward filling the green gap

Spontaneous Self-Assembly of Perovskite Nanocrystals into Electronically Coupled Supercrystals: Toward Filling the Green Gap

Yu Tong, En-Ping Yao, Aurora Manzi, Eva Bladt, Kun Wang, Markus Döblinger, Sara Bals, Peter Müller-Buschbaum, Alexander S. Urban, Lakshminarayana Polavarapu, and Jochen Feldmann*

Yu Tong, Dr. En-Ping Yao, Aurora Manzi, Dr. Alexander S. Urban, Dr. Lakshminarayana Polavarapu, Prof. Dr. Jochen Feldmann
Chair for Photonics and Optoelectronics, Department of Physics and Center for NanoScience (CeNS), Ludwig-Maximilians-Universität München, Amalienstr. 54, 80799 Munich, Germany
Nanosystems Initiative Munich (NIM), Schellingstr. 4, 80799 Munich, Germany
Email: l.polavarapu@lmu.de

Kun Wang, Prof. Dr. Peter Müller-Buschbaum
Technische Universität München, Physik-Department, Lehrstuhl für Funktionelle Materialien, James-Franck-Str. 1, 85748 Garching, Germany
Nanosystems Initiative Munich (NIM), Schellingstr. 4, 80799 Munich, Germany

Dr. Eva Bladt, Prof. Sara Bals
EMAT, University of Antwerp, Groenenborgerlaan 171, B-2020 Antwerp, Belgium

Dr. Markus Döblinger
Department of Chemistry, Ludwig-Maximilians-Universität München, Munich, Germany

KEYWORDS: $CsPbX_3$ perovskite, Supercrystals, Superlattices, Electronic coupling, Green LEDs.

ABSTRACT: Self-assembly of nanoscale building blocks into ordered nanoarchitectures has emerged as a simple and powerful approach for tailoring the nanoscale properties and the opportunities of using these properties for the development of novel optoelectronic nanodevices. Here, we report on the one-pot synthesis of $CsPbBr_3$ perovskite supercrystals (SCs) in a colloidal dispersion by ultrasonication. The growth of the SCs occurs through the spontaneous self-assembly of individual nanocrystals (NCs), which form in highly-concentrated solutions of precursor powders. The SCs retain the high photoluminescence (PL) efficiency of their NC subunits, however also exhibit a redshifted emission wavelength compared to that of the individual nanocubes due to inter-particle electronic coupling. This redshift makes the SCs pure green emitters with PL maxima at ~ 530-535 nm, while the individual nanocubes emit a cyan-green color (~512 nm). The SCs can be used as an emissive layer in the fabrication of pure green LEDs on rigid or flexible substrates. Moreover, the PL emission color is tunable across the visible range by employing a well-established halide ion exchange reaction on the obtained $CsPbBr_3$ SCs. These results highlight the promise of perovskite SCs for light emitting applications, while providing insight into their collective optical properties.

Recently, metal halide perovskites have created a great deal of excitement especially for solar energy conversion applications based on their outstanding optical and optoelectronic properties.[1-7] Consequently, this promising material has been explored for many uses, such as light-emitting devices (LEDs), lasers, photodetectors and photovoltaics.[8-10] For light emission, it has been shown that lower dimensional NCs provide far superior performances and tunability than their bulk counterparts.[11-18] In particular, colloidal cesium lead halide ($CsPbX_3$, X=Cl, Br and I) perovskite NCs have shifted to the center of attention as they exhibit higher stability as well as extremely high PL quantum yields (~80-100%) compared to organic-inorganic hybrid perovskites.[8, 19-21] The optical properties of perovskite NCs are generally tunable across the entire visible range by controlling the halide composition[22-24] and dimensionality.[24-26] Many groups have also been investigating a wide range of morphologies such as nanocubes, nanoplatelets and nanowires in order to determine their effect on the optical properties of the NCs.[26-31] Despite the rapid advances of low dimensional $CsPbBr_3$ perovskite NCs, achieving a pure green emission with high quantum efficiency is still challenging. Generally, the NCs are employed as phosphors, absorbing blue light emitted from a solid state LED and emitting in the yellow or green and red to replicate white light.[32, 33] Also, while they typically far outperform the bulk thin films in terms of light emission, they are only weakly emitting in the blue and currently cannot replicate a true green emission, which would be essential for closing the so-called "green gap".[24, 34, 35]

One of the reasons for the reduced quantum yield (QY) in bulk structures lies in the nature of the long diffusion length of charge carriers in perovskites. Once created they have a large chance of diffusing to a trap state in the crystal and undergoing subsequent non-radiative recombination.[31] One possibility to work around this problem could be to start with high PLQY nanocrystals and couple them together electronically. The electronic coupling, while leading to a redshift of the PL, could limit the diffusion length of the carriers, thereby significantly reducing the probability for trap-assisted recombination. This can be achieved through the self-assembly of NCs into SCs/superlattices, exhibiting a miniband formation in both valance and conduction bands.[36-39] Such miniband formation has been observed previously in conventional semiconductors such as GaAs superlattices[36] and aggregated CdTe nanocrystals,[39] however it has yet to be realized in perovskites. The self-assembly process itself, which has been extensively used to control the properties of metal, magnetic and conventional semiconductor NCs, presents an interesting way of bringing the NCs together in such a desired manner.[40-45] This process is typically accomplished by several methods: 1) slow solvent evaporation of the concentrated colloidal NC solution on a solid substrate, 2) via self-assembly at air/liquid or liquid/liquid interfaces, and 3) through intermolecular interactions between ligands of the NC surface. Importantly, the morphology and monodispersity of NCs play a crucial role in the formation of ordered assemblies. Despite significant advances in the self-assembly of metal and conventional semiconductor NCs into

one, two and three-dimensional (1D, 2D and 3D) superlattices,[40-44] very few attempts have been made to date toward the realization of perovskite self-assemblies and understanding their ensemble properties. [2, 31, 46]

Herein, we report on the spontaneous self-assembly of $CsPbBr_3$ perovskite NCs into highly luminescent colloidal 3D SCs in a one-pot colloidal synthesis from a concentrated precursor solution. It was found that the SCs exhibit a redshifted emission compared to the fluorescence of individual $CsPbBr_3$ NCs due to interparticle electronic coupling, yet retain the high PL quantum yields of the individual NCs. The redshift makes the SCs pure green emitters (530-535 nm), while the individual $CsPbBr_3$ NCs exhibit only blue-green emission (510-515 nm). This is particularly promising for television display applications as per Rec. 2020 color standards. The emission color of SCs can be tuned across the visible light spectrum by varying the halide ion (Br, Cl^- and I^-) composition through typical halide ion exchange reaction.[22, 23] We demonstrate the applicability of the SCs by fabricating pure green electroluminescent devices (~530 nm).

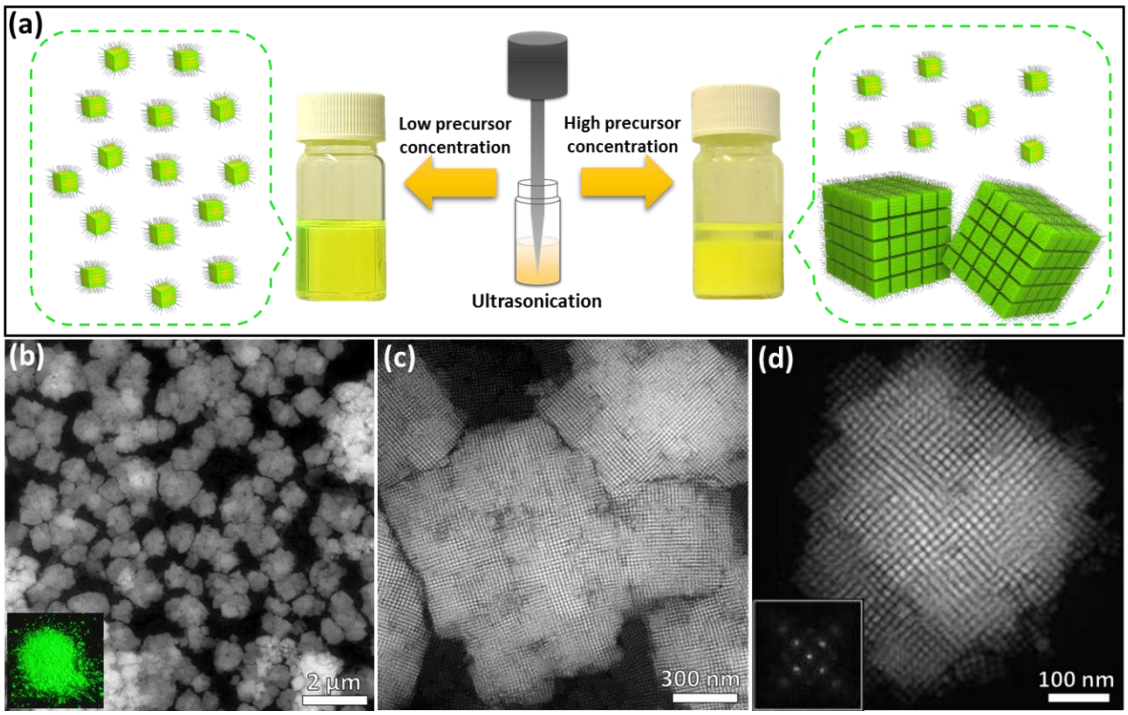

Figure 1: (a) Schematic illustration of the synthesis of $CsPbBr_3$ perovskite NCs by single-step tip sonication of precursor salts in octadecene in the presence of oleic acid and oleylamine. The reaction yields well-dispersed individual NCs at low precursor concentration (left side), while it results in the formation of self-assembled SCs for high precursor concentrations (right side). (b, c) HAADF-STEM images of the colloidal SCs with different magnifications. (Inset of b: photograph of SC powder under UV light illumination) (d) Magnified HAADF-STEM image of a single $CsPbB_3$ perovskite SC (inset: selected area FFT pattern of the SC).

The synthesis was based on findings from our previous study, in which perovskite NCs were synthesized directly from precursor salts by ultrasonication.[24] In the current work, we added the precursor salts (Cs_2CO_3 and $PbBr_2$) to octadecene in the presence of oleic acid

and oleylamine, however increased their concentration by ten times (Figure 1a, Figure S1). While the solution color turned into bright yellow, as in the case of the formed NCs, the solution became opaque and quickly, perovskite material precipitation was observed on the bottom of the vials, indicating the presence of large particles. To investigate this, we fully precipitated the dispersion, obtaining a yellow powder exhibiting a strong green emission when excited with UV light of 367 nm wavelength (inset of Figure 1b & S1). This is in contrast to common bulk-like perovskite crystals, which typically only show weak emission.[25] We then employed high angle annular dark field scanning transmission electron microscopy (HAADF-STEM) and were able to image particles several hundreds of nanometers in size (Figure 1b), thus explaining the observed precipitation. However, under closer inspection it turned out that these were not single large crystals, but were actually comprised of smaller cubic NCs roughly 10 nm in size (Figure 1c, d, and S2). This could be seen more clearly in a HAADF-STEM image acquired at a higher magnification, also revealing a typical spacing of 0.75-1.5 nm between the NCs (Figure 1d). A fast Fourier transformation (FFT) of the image clearly represents the cubic close packing of the crystalline nanocubes in these large crystal superlattices (Figure 1d). The polyhedral nature of these 200-400 nm large SCs could be observed nicely in scanning electron microscopy images (SEM), although care had to be given to prevent the structures from degrading under the electron beam (Figure S3).[25, 47] In addition, X-ray diffraction (XRD) of the individual $CsPbBr_3$ NCs and of the SCs revealed similar diffraction patterns, which can be assigned to either cubic or orthorhombic crystal structures (Figure S4). The clearer peaks from the SCs are likely due to the larger concentration of material in the measured powders.

In addition to 3D SCs, we also observed some self-assembled monolayers of $CsPbBr_3$ nanocubes in the STEM images (Figure S2). These monolayers likely form spontaneously during the drying process from individual NCs present in the concentrated colloidal dispersion. In fact this process has been widely enforced to obtain large-area 2D and 3D self-assemblies of metal and semiconductor NCs on solid surfaces. In contrast, the spontaneous self-assembly of NCs into well-defined SCs in colloidal dispersions has only been rarely observed.[48, 49] The self-assembly process of the SCs in the dispersions is likely governed by the van der Waals attraction between the hydrophobic ligands and the perovskite NC cores under high colloidal concentration. Such spontaneous self-assembly processes have been previously observed in the formation of free-standing SCs of polyhedral gold NCs.[49]

In order to elucidate the formation process of the perovskite SCs out of the precursor powders, we monitored the PL spectra of the reaction product during the synthesis (Figure 2a). Images of the vials illuminated with white light can be found in the Supporting Information (Figure S1). For the first 5 minutes, there is only little if any PL observable. At 5 minutes we observe a broad PL signal, with distinct shoulders at 499 nm and 526 nm. While the latter peak corresponds to the PL emission of bulk $CsPbBr_3$, the former peak likely stems from smaller NCs exhibiting quantum-confinement. As the reaction progresses, the shoulder decreases in intensity and redshifts up to 512 nm, becoming nearly indistinguishable at 30 min. This value corresponds to that seen previously for weakly confined $CsPbBr_3$ NCs.[24, 50, 51] The main peak gradually redshifts to 535 nm during the course of the synthesis. This was quite surprising as the reported PL maxima for $CsPbBr_3$ NCs exhibit a maximum wavelength of 520 nm, even for non-quantum confined NCs (sizes >10 nm).[14, 24] It instead resembles that of bulk macrocrystals of $CsPbBr_3$[38] and thin films.[52]

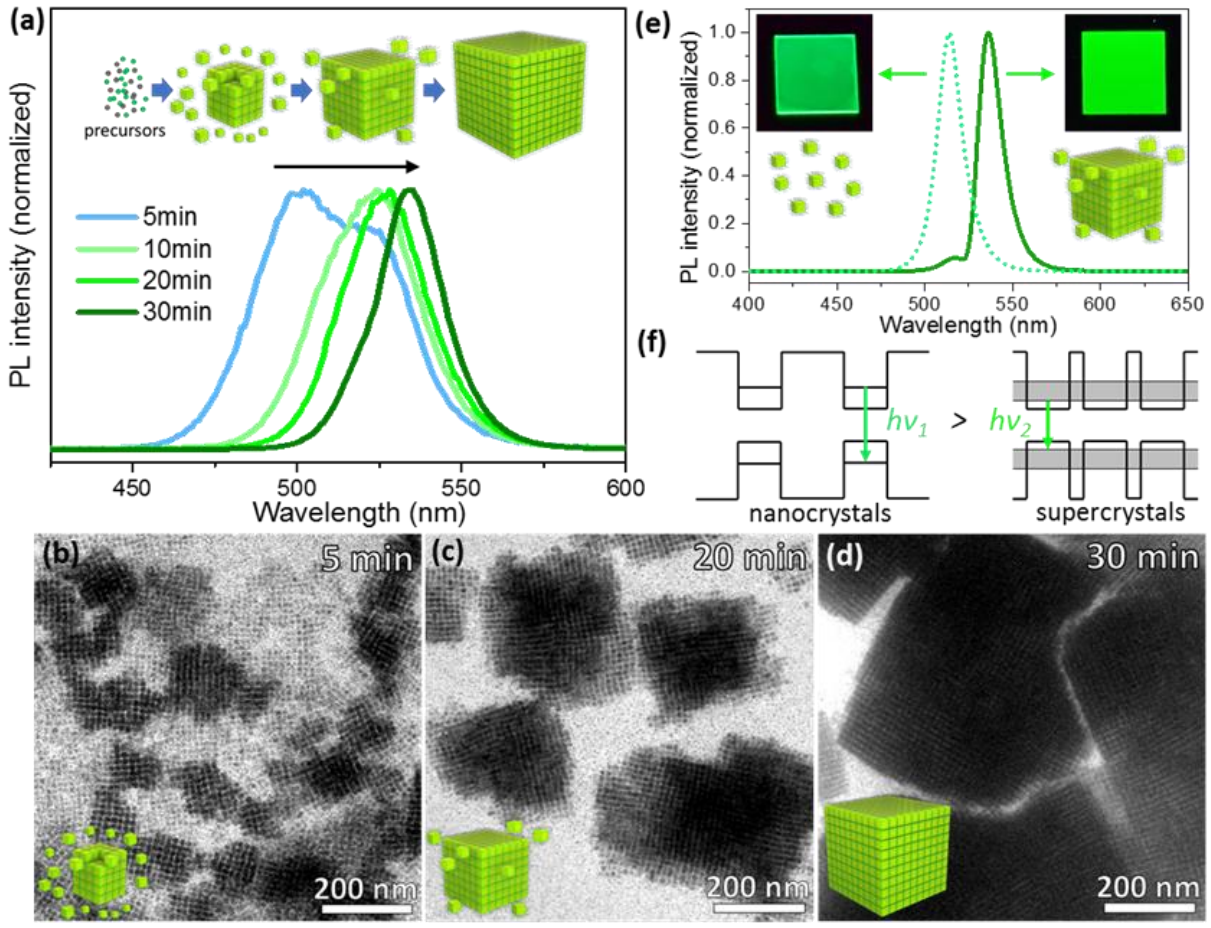

Figure 2: (a) PL spectra of the CsPbBr3 perovskite colloidal dispersion obtained at different reaction times during the transformation of precursor powders into SCs by ultrasonication. Inset: Schematic illustration of the gradual transformation of precursor powders into 3D SCs of CsPbBr3 nanocubes. (b-d) BF-TEM images of the crystals present after 5, 20, and 30 minutes of synthesis time. (e) PL spectra of perovskite films of individual NCs (left side) and SCs (right side). Insets are photos of the films under UV-light illumination. (f) Energy diagram of the corresponding situations. While the NCs remain electronically isolated (left

side), the individual NCs inside the SCs couple together leading to miniband formation and a redshift of the emission wavelength.

To understand the origin of these spectra, we acquired bright field transmission electron microscopy (BF-TEM) images on material extracted from the synthesis at specific times during the synthesis (Figure 2b-d). After 5 min many individual NCs can be seen along with some smaller clusters with largest contrast, indicating the formation of small SCs. As the synthesis progresses, the single NCs vanish, being replaced by larger and larger SCs, with an increasing contrast consistent with their increasing lateral sizes. Thus the redshift of the PL spectra is concomitant with the increase in the SC size. Interestingly, upon dilution of these SC dispersions, the PL position blueshifts again, nearly to the position of the NCs formed under lower concentrations (Figure S5a). TEM imaging confirms that the dilution leads to a splits up of the SCs, resulting in predominantly separated NCs with a few small NC aggregates dispersed in between (Figure S5c, d). The difference in emission wavelength can be seen even more clearly in PL spectra acquired from dense films fabricated from the NCs and SCs (Figure 2e). The PL is redshifted by 21 nm to 535 nm for the SC film, with a small shoulder remaining at 516, and likely stemming from single NCs present in the SC dispersion. Since the NCs basically remain separated instead of fusing together, the observed shift must stem from an electronic coupling between the individual NCs. Possibilities for such coupling have been studied in literature previously, although often on SCs of epitaxially grown quantum dots.[36, 37, 53] In a similar way as the atoms interact in an atomic solid, the electronic wavefunctions of the individual semiconductor NCs can interact strongly in a perovskite SC, provided a small enough spacing, which in turn can lead to the formation of minibands in both valence and conduction bands, as illustrated in Figure 2f.[36] Such miniband formation in SCs leads to a lowering of the lowest-energy optical transition, which is seen in the redshift of the PL as compared with individual NCs.[39] Studies on two-dimensional perovskites show that miniband formation should be observable at separation distances comparable to those obtained for the supercrystals.[54] Previous studies have shown that the red-shift in the PL emission of perovskites can also be caused by reabsorption.[55] However, reabsorption only affects the PL and not the absorption (or PLE), as initially emitted photons are reabsorbed with subsequently emitted photons being redshifted to the originally emitted ones. This leads to a narrowing of the PL signal with a reduction on the short wavelength side and a concomitant increase on the long wavelength side. In our case, we observe a strong redshift of the PLE onset from the NCs to the SCs accompanied by a similar redshift of the PL signal (see Figure S6). As the width of the PL peaks are nearly identical, we can rule out reabsorption as a major effect in our system. In addition, the results show that the redshift in the PL peak position is quite significant at the initial stages of the SC growth. As the number of NCs in the SCs increases, the redshift only increases slightly (Figure 2a). This is due to the fact that electronic coupling is significant only among nearest neighbors.

In addition, it is worth mentioning that it was easy to prepare films of SCs compared to the films made of uncoupled NCs, because of the high concentration of colloids in SC dispersion. The another reason for this is that the purification of SCs by centrifugation is a lot easier due to their heavy mass, where as it was difficult to separate the excess ligands from the well-dispersed NCs. The SCs can be prepared in high concentration colloidal dispersion for its use in the fabrication of dense films by spin-coating. The PL emission wavelength of the films made of SCs greatly depends on the concentration of the colloidal solution used for their fabrication (Figure S7). If the solutions are diluted before spin-coating, the SCs disassemble, resulting in a blueshift of the PL emission peak. More importantly, despite the SCs being highly purified, with nearly no residual ligand remaining in the dispersions, the films made of SCs are highly emissive with a PLQY of 45 %, even slightly surpassing that of the NC films, which exhibited a PLQY of ~40%. The quantum yield in the films is lower than in the dispersions. This is likely due to partial ligand desorption, which occurs during the rigorous purification which is necessary to obtain high quality films. Apparently, the self-assembly of NCs into SCs is not detrimental on the PLQY. This is extremely interesting, as both films comprising larger NCs (~100 nm) and bulk thin films exhibited extremely low PLQYs of 0.5% and <0.1%, respectively (Figure S8). Thus, the redshifted emission typical of bulk-sized CsPbBr3 perovskite structures can be merged together with the superior QY of weakly-confined NCs in the SCs. These superior properties of SCs make them unique for light emitting applications, as compared with bulk films.

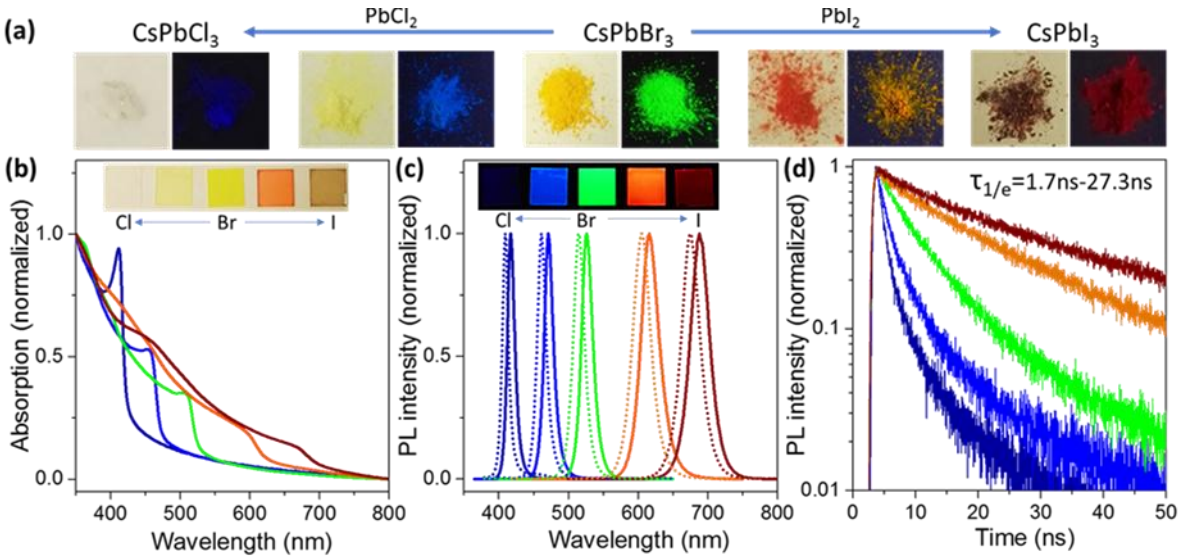

Figure 3: (a) Photographs of the powders of $CsPbX_3$ perovskite SCs with different halide compositions under room light (left side) and UV light illumination (right side). (b) UV/Vis absorption spectra of perovskite films made by spin-coating concentrated colloidal dispersion diluted colloidal SC dispersions. (c) The corresponding PL spectra (solid line) in comparison with those of films of isolated NCs. (Insets of figures (b) and (c): photographs of the perovskite SC films under room light and UV illumination, respectively). (d) PL decay dynamics of the SC films shown in (c). The PL lifetime increases with increasing emission wavelength from 1.7 ns to 27.3 ns.

The commonly used method of halide ion exchange to shift the optical bandgap and PL emission of perovskite NCs is easily applicable to the SCs (Figure 3a, Figure S9).[22, 23] Similarly to the bromide case, strongly luminescing powders can be obtained with a clear color difference depending on halide content. The ion exchange process turned out to be significantly slower than for the individual NC dispersion, likely due to the halide ions having to permeate the dense SCs in order to replace the original halide ions for all NCs. Importantly, the halide ion exchange reaction basically preserves the SC morphology as confirmed by TEM characterization (Figure S10) despite a partial disassembly of the SCs upon dilution in the solutions required for ion exchange. As shown in Figure 3b,c, the absorption onset and PL emission peaks of films fabricated out of the $CsPbX_3$ SCs gradually blue-shift with increasing chloride amount and redshift as the iodide content increases. The PL spectra of all colloidal perovskite SCs (solid lines) show the same redshift in comparison to the individual NC solutions (dashed lines), so that they likely all exhibit electronic coupling. The SC films containing Br and I ions exhibit relatively high PLQYs around 45%, whereas the Cl-containing samples exhibit low PLQYs of around 10%. Time-resolved PL measurements revealed an inverse correlation between the lifetime and halide ion-controlled band gap, as previously reported by us and others for individual perovskite NCs.[1, 24]

These results suggest that the SCs can be employed for integration into optoelectronic devices due to their excellent optical properties, high yield and stability.

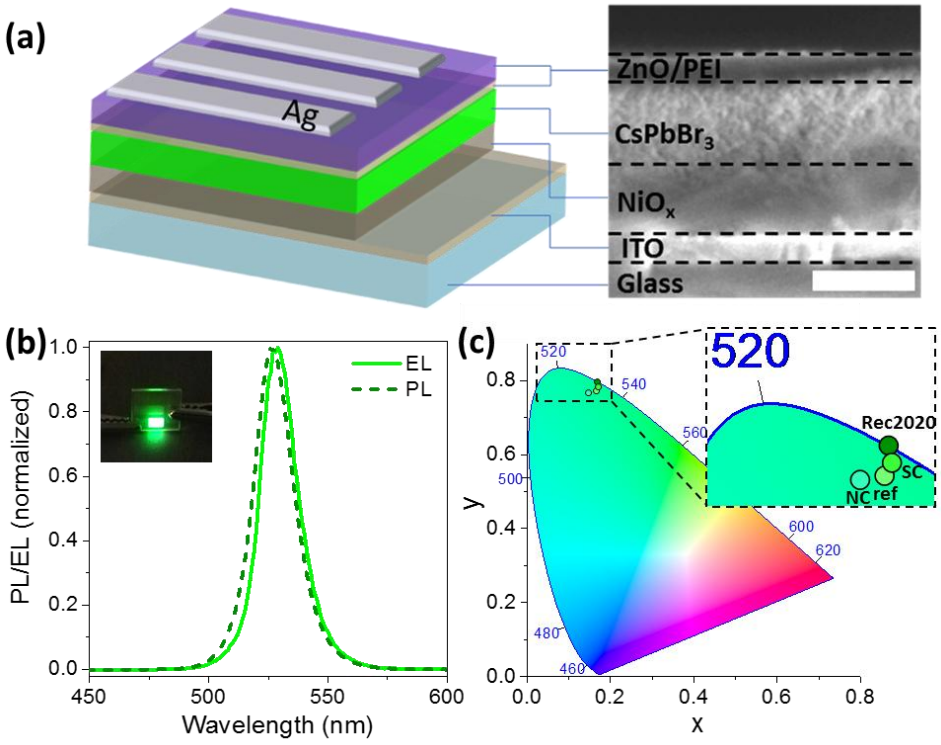

Figure 4: (a) Device architecture and cross-sectional SEM image of the $CsPbBr_3$ perovskite LED device. (b) The electroluminescence and PL spectra of the $CsPbBr_3$ perovskite SC (insets: photograph of the corresponding LED device showing EL). (c) CIE coordinates of the

SC LED device (inset: Magnified view of the color coordinates of $CsPbBr_3$ SCs (SC), isolated NCs of $CsPbBr_3$ (NC) and $FAPbBr_3$ (ref) in comparison with the recommended pure green (Rec2020) color.

One problem in thin film LEDs is currently the lack of a true green emitter with high quantum yield. This dearth has been dubbed the "green gap".[34] $CsPbBr_3$ NCs have proven to be promising materials for light emitting application owing to their facile synthesis with high PLQY. The number of research articles is increasing, which focused on the fabrication and optimization of perovskite LEDs based either on $CsPbBr_3$ thin films or NCs.[7, 8, 56] While the thin films show a color spectrum close to the desired Rec2020 standard, they exhibit low PLQYs (Figure S9). The bromide-based NCs on the other hand have quite high efficiencies, however, due to a weak quantum confinement, their emission color is shifted further away from the desired region.[10, 24, 57] As shown in this work, the $CsPbBr_3$ perovskite SCs exhibit an emission wavelength further shifted toward the recommended green (Rec2020) color. Hence, we now explore the fabrication of pure green LEDs on both rigid as well as on flexible substrates using the SCs as the emitting layer. One of the advantages of using perovskites in LEDs is the ability to use solution process. This means that the active layers can be deposited via spin-coating the corresponding solution, providing a simple and cost-effective approach for fabricating LEDs. In most previous studies on perovskite NC-based LEDs, the carrier transport layers on top of perovskite nanocrystal films were deposited via thermal evaporation, because the NCs are easily washed away by organic solvents if they are not properly cross-linked.[58] Here, we have successfully employed a solution-processed electron transport layer poly(ethyleneimine) (PEI)/ZnO on top of the perovskite film without affecting the perovskite SCs film using ZnO dispersed in ethyl acetate instead of toluene. The schematic illustration of the fabricated LED device architecture and the SEM image of the corresponding device cross section are presented in Figure 4a (see Figure S11 for top-view images of the individual layers**)**. An extremely thin PEI layer was introduced by spin-coating for stabilizing the perovskite layer as well as modifying the work function of ZnO.[59] The fabricated LED displays bright PL at 527 nm and a strong bright green electroluminescence (EL) at 3V, slightly redshifted to 529 nm (a photo is inset in Figure 4b). These peaks are only slightly blue-shifted from the SC film emission position of 536 nm due to the partial disassembly of SCs in the diluted solution used for spin-coating (Figure S7). A corresponding version of this LED, but using isolated $CsPbBr_3$ NCs was fabricated and showed the expected blue-shifted EL emission (Figure S12). The SC based EL device shows stable EL, with a gradual increase in intensity with increasing driving voltage up to 7V, while nearly retaining the peak position (Figure S13). As can be seen in Figure 4c, which is based on the CIE (International Commission on Illumination) 1931 color coordinator, the SC-based LED exhibits a color closer to the recommended pure green (Rec2020), in comparison to the $CsPbBr_3$ NC LED and also to that of a device based on formamidinium lead bromide

($FAPbBr_3$) NCs.[60] We also fabricated flexible LEDs on PET film instead of glass substrate using both NCs and SCs (Figure S14). This worked for both the NCs and SCs and the devices showed similar characteristics to those employing the rigid substrates. Together, these results highlight the promise of using perovskite SCs for display applications.

In summary, we have presented the spontaneous self-assembly of perovskite NCs into highly emissive SCs from precursor powders in a highly concentrated solution. Both steps, NC synthesis and self-assembly take place simultaneously in one pot. We have found that the perovskites SCs exhibit a redshifted PL emission due to electronic coupling of the wave functions in neighboring NCs and the resulting formation of mini-bands. The redshift in the PL of $CsPbBr_3$ SCs makes them pure green emitters, which is demonstrated by the fabrication of green EL-LED devices on rigid and even flexible substrates. Importantly, despite the more bulk-like emission wavelength, the SCs retain the high PL quantum yield of the NCs. The optical properties of the perovskite SCs are tunable across the visible spectrum by applying the common halide ion exchange reaction on the $CsPbBr_3$ SC-templates. The results presented in this work show the promise of the colloidal solution of SCs for solution-processed light emitting applications.

Supporting Information

Supporting Information is available from the Wiley Online Library or from the author.

Acknowledgements

This research work was supported by the Bavarian State Ministry of Science, Research, and Arts through the grant "Solar Technologies go Hybrid (SolTech)," by the China Scholarship Council (Y.T. and K.W.), by the European Union's Horizon 2020 research and innovation program under the Marie Skłodowska-Curie Grant Agreement COMPASS No. 691185 and by LMU Munich's Institutional Strategy LMUexcellent within the framework of the German Excellence Initiative (L.P. and A.S.U). E.B. and S.B. acknowledge financial support from the European Research Council (ERC Starting Grant #335078-COLOURATOMS).

References

[1] L. Protesescu, S. Yakunin, M. I. Bodnarchuk, F. Krieg, R. Caputo, C. H. Hendon, R. X. Yang, A. Walsh, M. V. Kovalenko, *Nano Lett.* **2015**, *15*, 3692.
[2] M. V. Kovalenko, L. Protesescu, M. I. Bodnarchuk, *Science* **2017**, *358*, 745.
[3] L. Dou, A. B. Wong, Y. Yu, M. Lai, N. Kornienko, S. W. Eaton, A. Fu, C. G. Bischak, J. Ma, T. Ding, N. S. Ginsberg, L.-W. Wang, A. P. Alivisatos, P. Yang, *Science* **2015**, *349*, 1518.
[4] S. D. Stranks, G. E. Eperon, G. Grancini, C. Menelaou, M. J. P. Alcocer, T. Leijtens, L. M. Herz, A. Petrozza, H. J. Snaith, *Science* **2013**, *342*, 341.
[5] G. Xing, N. Mathews, S. Sun, S. S. Lim, Y. M. Lam, M. Grätzel, S. Mhaisalkar, T. C. Sum, *Science* **2013**, *342*, 344.

[6] Q. A. Akkerman, M. Gandini, F. Di Stasio, P. Rastogi, F. Palazon, G. Bertoni, J. M. Ball, M. Prato, A. Petrozza, L. Manna, *Nat. Energy* **2016**, *2*, 16194.
[7] Y. Zhang, J. Liu, Z. Wang, Y. Xue, Q. Ou, L. Polavarapu, J. Zheng, X. Qi, Q. Bao, *Chem. Commun.* **2016**, *52*, 13637.
[8] H. Huang, L. Polavarapu, J. A. Sichert, A. S. Susha, A. S. Urban, A. L. Rogach, *NPG Asia Mater.* **2016**, *8*, e328.
[9] Y. Wang, X. Li, J. Song, L. Xiao, H. Zeng, H. Sun, *Adv. Mater.* **2015**, *27*, 7101.
[10] L. Polavarapu, B. Nickel, J. Feldmann, A. S. Urban, *Adv. Energy Mater.* **2017**, *7*, 1700267
[11] X. Li, Y. Wang, H. Sun, H. Zeng, *Adv. Mater.* **2017**, *29*, 1701185
[12] L. C. Schmidt, A. Pertegas, S. Gonzalez-Carrero, O. Malinkiewicz, S. Agouram, G. M. Espallargas, H. J. Bolink, R. E. Galian, J. Perez-Prieto, *J. Am. Chem. Soc.* **2014**, *136*, 850.
[13] A. Swarnkar, V. K. Ravi, A. Nag, *ACS Energy Lett.* **2017**, *2*, 1089.
[14] A. Swarnkar, R. Chulliyil, V. K. Ravi, M. Irfanullah, A. Chowdhury, A. Nag, *Angew. Chem. Int. Ed.* **2015**, *54*, 15424.
[15] J. Liu, Y. Xue, Z. Wang, Z.-Q. Xu, C. Zheng, B. Weber, J. Song, Y. Wang, Y. Lu, Y. Zhang, Q. Bao, *ACS Nano* **2016**, *10*, 3536.
[16] F. Zhang, H. Zhong, C. Chen, X.-g. Wu, X. Hu, H. Huang, J. Han, B. Zou, Y. Dong, *ACS Nano* **2015**, *9*, 4533.
[17] H. Huang, F. Zhao, L. Liu, F. Zhang, X.-g. Wu, L. Shi, B. Zou, Q. Pei, H. Zhong, *ACS Appl. Mater. Interfaces* **2015**, *7*, 28128.
[18] M. C. Weidman, M. Seitz, S. D. Stranks, W. A. Tisdale, *ACS Nano* **2016**, *10*, 7830.
[19] X. Zhang, H. Lin, H. Huang, C. Reckmeier, Y. Zhang, W. C. H. Choy, A. L. Rogach, *Nano Lett.* **2016**, *16*, 1415.
[20] M. Chen, Y. T. Zou, L. Z. Wu, Q. Pan, D. Yang, H. C. Hu, Y. S. Tan, Q. X. Zhong, Y. Xu, H. Y. Liu, B. Q. Sun, Q. Zhang, *Adv. Funct. Mater.* **2017**, *27*.
[21] Y. Bekenstein, B. A. Koscher, S. W. Eaton, P. D. Yang, A. P. Alivisatos, *J. Am. Chem. Soc.* **2015**, *137*, 16008.
[22] G. Nedelcu, L. Protesescu, S. Yakunin, M. I. Bodnarchuk, M. J. Grotevent, M. V. Kovalenko, *Nano Lett.* **2015**, *15*, 5635.
[23] Q. A. Akkerman, V. D'Innocenzo, S. Accornero, A. Scarpellini, A. Petrozza, M. Prato, L. Manna, *J. Am. Chem. Soc.* **2015**, *137*, 10276.
[24] Y. Tong, E. Bladt, M. F. Aygüler, A. Manzi, K. Z. Milowska, V. A. Hintermayr, P. Docampo, S. Bals, A. S. Urban, L. Polavarapu, J. Feldmann, *Angew. Chem. Int. Ed.* **2016**, *55*, 13887.
[25] J. A. Sichert, Y. Tong, N. Mutz, M. Vollmer, S. Fischer, K. Z. Milowska, R. García Cortadella, B. Nickel, C. Cardenas-Daw, J. K. Stolarczyk, A. S. Urban, J. Feldmann, *Nano Lett.* **2015**, *15*, 6521.
[26] V. A. Hintermayr, A. F. Richter, F. Ehrat, M. Döblinger, W. Vanderlinden, J. A. Sichert, Y. Tong, L. Polavarapu, J. Feldmann, A. S. Urban, *Adv. Mater.* **2016**, *28*, 9478.
[27] Y. Tong, F. Ehrat, W. Vanderlinden, C. Cardenas-Daw, J. K. Stolarczyk, L. Polavarapu, A. S. Urban, *ACS Nano* **2016**, *10*, 10936.
[28] Q. A. Akkerman, S. G. Motti, A. R. Srimath Kandada, E. Mosconi, V. D'Innocenzo, G. Bertoni, S. Marras, B. A. Kamino, L. Miranda, F. De Angelis, A. Petrozza, M. Prato, L. Manna, *J. Am. Chem. Soc.* **2016**, *138*, 1010.
[29] Y. Bekenstein, B. A. Koscher, S. W. Eaton, P. Yang, A. P. Alivisatos, *J. Am. Chem. Soc.* **2015**, *137*, 16008.
[30] D. Zhang, S. W. Eaton, Y. Yu, L. Dou, P. Yang, *J. Am. Chem. Soc.* **2015**, *137*, 9230.
[31] Y. Tong, B. J. Bohn, E. Bladt, K. Wang, P. Müller-Buschbaum, S. Bals, A. S. Urban, L. Polavarapu, J. Feldmann, *Angew. Chem. Int. Ed.* **2017**, *56*, 13887.

[32] H. Huang, B. Chen, Z. Wang, T. F. Hung, A. S. Susha, H. Zhong, A. L. Rogach, *Chem. Sci.* **2016**, *7*, 5699.
[33] S. Pathak, N. Sakai, F. Wisnivesky Rocca Rivarola, S. D. Stranks, J. Liu, G. E. Eperon, C. Ducati, K. Wojciechowski, J. T. Griffiths, A. A. Haghighirad, A. Pellaroque, R. H. Friend, H. J. Snaith, *Chem. Mater.* **2015**, *27*, 8066.
[34] F. Nippert, S. Y. Karpov, G. Callsen, B. Galler, T. Kure, C. Nenstiel, M. R. Wagner, M. Straßburg, H.-J. Lugauer, A. Hoffmann, *Appl. Phys. Lett.* **2016**, *109*, 161103
[35] I. Lignos, L. Protesescu, D. B. Emiroglu, R. Maceiczyk, S. Schneider, M. V. Kovalenko, A. J. deMello, *Nano Lett.* **2018**, *18*, 1246
[36] T. Sugaya, T. Amano, M. Mori, S. Niki, *Appl. Phys. Lett.* **2010**, *97*, 043112.
[37] M. Scheibner, T. Schmidt, L. Worschech, A. Forchel, G. Bacher, T. Passow, D. Hommel, *Nat. Phys.* **2007**, *3*, 106.
[38] Y. Rakita, N. Kedem, S. Gupta, A. Sadhanala, V. Kalchenko, M. L. Böhm, M. Kulbak, R. H. Friend, D. Cahen, G. Hodes, *Cryst. Growth and Design* **2016**, *16*, 5717.
[39] J. Zhang, A. A. Lutich, A. S. Susha, M. Döblinger, C. Mauser, A. O. Govorov, A. L. Rogach, F. Jäckel, J. Feldmann, *J. Appl. Phys.* **2010**, *107*, 123516.
[40] Z. Nie, A. Petukhova, E. Kumacheva, *Nat. Nanotech.* **2009**, *5*, 15.
[41] C. R. Kagan, C. B. Murray, *Nat. Nanotech.* **2015**, *10*, 1013.
[42] M. P. Pileni, *J. Phys. Chem. B* **2001**, *105*, 3358.
[43] Y. Min, M. Akbulut, K. Kristiansen, Y. Golan, J. Israelachvili, *Nat. Mater.* **2008**, *7*, 527.
[44] L. Motte, F. Billoudet, E. Lacaze, M.-P. Pileni, *Adv. Mater.* **1996**, *8*, 1018.
[45] M. Grzelczak, J. Vermant, E. M. Furst, L. M. Liz-Marzán, *ACS Nano* **2010**, *4*, 3591.
[46] N. Soetan, W. R. Erwin, A. M. Tonigan, D. G. Walker, R. Bardhan, *J. Phys. Chem. C* **2017**, *121*, 18186.
[47] Z. Dang, J. Shamsi, F. Palazon, M. Imran, Q. A. Akkerman, S. Park, G. Bertoni, M. Prato, R. Brescia, L. Manna, *ACS Nano* **2017**, *11*, 2124.
[48] L.-X. Dai, X.-Y. Wang, X.-Y. Zheng, Y.-W. Zhang, *Chem. Commun.* **2016**, *52*, 5023.
[49] C.-W. Yang, C.-Y. Chiu, M. H. Huang, *Chem. Mater.* **2014**, *26*, 4882.
[50] L. Protesescu, S. Yakunin, M. I. Bodnarchuk, F. Krieg, R. Caputo, C. H. Hendon, R. X. Yang, A. Walsh, M. V. Kovalenko, *Nano Lett.* **2015**, *15*, 3692.
[51] D. N. Dirin, I. Cherniukh, S. Yakunin, Y. Shynkarenko, M. V. Kovalenko, *Chem. Mater.* **2016**, *28*, 8470.
[52] Y. Li, Z.-F. Shi, S. Li, L.-Z. Lei, H.-F. Ji, D. Wu, T.-T. Xu, Y.-T. Tian, X.-J. Li, *J. Mater. Chem. C* **2017**, *5*, 8355.
[53] D. V. Talapin, J.-S. Lee, M. V. Kovalenko, E. V. Shevchenko, *Chem. Rev.* **2010**, *110*, 389.
[54] J. Song, J. Li, X. Li, L. Xu, Y. Dong, H. Zeng, *Adv. Mater.* **2015**, *27*, 7162.
[55] L. Protesescu, S. Yakunin, M. I. Bodnarchuk, F. Bertolotti, N. Masciocchi, A. Guagliardi, M. V. Kovalenko, *J. Am. Chem. Soc.* **2016**, *138*, 14202.
[56] G. Li, F. W. R. Rivarola, N. J. L. K. Davis, S. Bai, T. C. Jellicoe, F. de la Peña, S. Hou, C. Ducati, F. Gao, R. H. Friend, N. C. Greenham, Z.-K. Tan, *Adv. Mater.* **2016**, *28*, 3528.
[57] S. Woo, W. Hyun Kim, H. Kim, Y. Yi, H.-K. Lyu, Y. Kim, *Adv. Energy Mater.* **2014**, *4*, 1301692
[58] S. Kumar, J. Jagielski, N. Kallikounis, Y.-H. Kim, C. Wolf, F. Jenny, T. Tian, C. J. Hofer, Y.-C. Chiu, W. J. Stark, T.-W. Lee, C.-J. Shih, *Nano Lett.* **2017**, *17*, 5277.

Table of contents

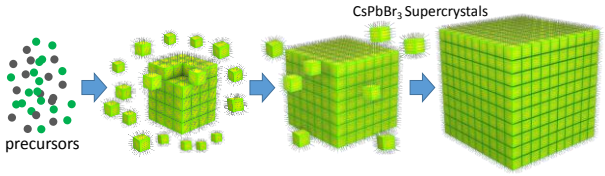

The synthesis and spontaneous self-assembly of perovskite nanocrystals (NCs) into supercrystals (SCs) at high colloid concentration takes place in one-pot, starting with precursor powders. The perovskite SCs exhibit redshifted photoluminescence (PL) peak due to interparticle electronic coupling. The SCs exhibit bulk like optical properties while maintaining the high PL quantum yields of NCs. Using the $CsPbBr_3$ SCs, we have demonstrated the fabrication of flexible LEDs with pure green emission.

Keyword: $CsPbX_3$ perovskite, Supercrystals, Superlattices, Electronic coupling, Green LEDs.

Yu Tong, En-Ping Yao, Aurora Manzi, Eva Bladt, Kun Wang, Markus Döblinger, Sara Bals, Peter Müller-Buschbaum, Alexander S. Urban, Lakshminarayana Polavarapu,* and Jochen Feldmann

Title: Spontaneous Self-assembly of Perovskite Nanocrystals into Electronically Coupled Supercrystals: Toward filling the Green Gap

Supporting information

Spontaneous Self-assembly of Perovskite Nanocrystals into Electronically Coupled Supercrystals: Toward filling the Green Gap

Yu Tong, En-Ping Yao, Aurora Manzi, Eva Bladt, Kun Wang, Markus Döblinger, Sara Bals, Peter Müller-Buschbaum, Alexander S. Urban, Lakshminarayana Polavarapu, and Jochen Feldmann*

Materials: Cs_2CO_3 (Cesium carbonate, 99%), $PbCl_2$ (lead (II) chloride, 98%), $PbBr_2$ (lead (II) bromide 98%), PbI_2 (lead (II) iodide 99%), 1-octadecene (technical grade 90%), oleic acid (technical grade 90%), oleylamine (technical grade 70%), acetone (HPLC, ≥99.8%), hexane (HPLC, grade ≥97.0%, GC), ethyl acetate (HPLC, ≥99.7%), nickel(II) nitrate hexahydrate ($Ni(NO_3)_2 \cdot 6H_2O$), ethylene glycol (reagent grade, ≥99.7%), ethylenediamine (≥99%), polyethylenimine (branched), zinc oxide nanoparticles dispersion (40 wt. % in butyl acetate) and LiF (Lithium fluoride, 99.99 were purchased from Sigma-Aldrich and used as received. The ZnO colloidal dispersion obtained from Sigma-Aldrich was diluted 10 times with ethyl acetate. PEDOT:PSS solution was purchased from Heraeus (Germany) and filtered before use. ITO glasses were purchased from SOLEMS (France), while the ITO coated PET flexible substrates were purchased from Solaronix (Switzerland). TPBi was purchased from Ossila (UK).

Synthesis of $CsPbBr_3$ supercrystals: The synthesis of $CsPbBr_3$ supercrystals (SCs) takes the merits of single-step ultrasonication assisted synthesis of perovskite nanocrystals (NCs), as reported in our previous work.[31, 61] In a typical synthesis, 10 ml of 1-octadecene, 1.5 ml of oleic acid and 1.5ml of oleylamine were added to a mixture of 1 mmol of Cs_2CO_3 and 3 mmol of $PbBr_2$ precursor powders in a 20 ml glass bottle. The resultant mixture was subjected to tip sonication (SONOPULS HD 3100, BANDELIN) at a power of 30 W for 30 minutes, as

shown in Figure S1.[61] During the sonication, the white color precursor powders dissolved in octadecene and the reaction mixture gradually transformed to yellow, indicating the formation of perovskite colloidal NCs. After 30 min of sonication, the reaction medium was cooled down to room temperature and then centrifuged at 6000 rpm for 15 min. The resultant sediment containing colloidal perovskite was dispersed in 3 ml of hexane for optical and morphological characterization. In order to obtain perovskite powders, the sediment was gently washed twice with hexane (to remove excess residual ligands) by centrifugation at 3000 rpm, and the obtained sediment was dried in air. It is worth to mention that the purification of SCs by centrifugation was easier due to their heavy mass as compared to isolated NCs.

Composition tuning through halide ion exchange: At first, the halide ion (Cl & I) precursor solutions were prepared by dissolving 0.3 mmol of $PbCl_2$ or PbI_2 powers in a mixture of 10 ml of hexane, 0.3 ml of oleylamine and 0.3 ml of oleic acid at 100 ^oC under continuous stirring, as reported in our previous work.[31] Then, the appropriate volume of halide (Cl & I) precursor solution was added to the as-synthesized $CsPbBr_3$ assemblies under vigorous stirring for 20 min. The halide ion exchange process can be clearly seen by the color change upon the addition of precursor solution. After the competition of ion exchange process, the SC colloids were purified by centrifugation at 6000 rpm for 15 min. The resultant sediment was dispersed in hexane for further characterization.

Preparation of bulk large size $CsPbBr_3$ colloidal crystals and thin films:

The bulk $CsPbBr_3$ colloidal crystals were also synthesized by optimizing the tip-sonication approach developed by our group.[31, 61] We have found that the size of the perovskite NCs increased by decreasing the concentration of ligand with respect to precursors. In typical synthesis, 10 ml of 1-octadecene, 0.5 ml of oleic acid and 0.5 ml of oleylamine were added to a mixture of 1 mmol of Cs_2CO_3 and 3 mmol of $PbBr_2$ precursor powders in a 20 ml glass bottle, followed by tip-sonication for 30 min. After completion of reaction, the product was

purified by centrifugation at 2000 rpm and the sediment was redispersed in hexane, yielding the $CsPbBr_3$ colloidal crystals. The purification process was repeated twice and the resultant sediment was dispersed in hexane for optical and morphological characterization. The bulk $CsPbBr_3$ film were prepared by annealing the NC film at 180 ^oC for 30 min, as reported previously.[62]

Fabrication of light emitting diodes (LEDs):

First of all, selected area of indium tin oxide (ITO) coated substrates were etched using hydrochloride acid and zinc powders. Then, the substrates were ultrasonically cleaned with detergent, deionized water, acetone, and isopropyl alcohol. The substrates were further cleaned with oxygen plasma treatment. The cleaned substrates were used for the fabrication of LEDs both on rigid and flexible substrates by two different process as discussed below.

a) Solution-processed method: The device architecture can be seen in Figure 4a. At first, NiO_x precursor (1M nickel (II) nitrate hexahydrate in ethylene glycol with 50 μl/ml ethylenediamine) was spin-coated on ITO substrates at 4000 rpm followed by annealing at 300°C for 1h, as described in the previous work.[63] Then, a 10-time diluted $CsPbBr_3$ perovskite SC or isolated $CsPbBr_3$ NC colloidal dispersion was spin-coated on top of NiO_x at 6000 rpm. Afterwards, the PEI solution (20mg/ml in acetone) was spin-coated at 4000rpm, followed by a subsequent spin-coating of ZnO NP colloid layer at 5000 rpm. The device fabrication ended with a thermal evaporation of Ag as cathode.
b) Flexible LEDs: The device architecture can be seen in Figure S13a. At first, PEDOT:PSS was spin-coated onto ITO coated PET substrate at 4000 rpm, and then annealed at 140°C for 20 min. Then, the colloidal SC or NC dispersion was spin-coated at 6000 rpm, followed by a thermal evaporation of TPBi, LiF, and Ag to complete the fabrication of flexible LEDs.

***Optical characterization*:** The extinction spectra of the samples were measured using Cary 5000 UV-Vis-NIR spectrophotometer. The absorption spectra were obtained by the same

instrument coupled with integrating sphere. The PL and PL quantum yield measurements were performed using Varian Cary Eclipse fluorescence spectrophotometer (Agilent Technologies) and Fluorolog-3 FL3-22 (Horiba Jobin Yvon GmbH) spectrometer equipped with an integrating sphere, respectively. Electroluminescence (EL) of the prepared LEDs were recorded using Fluorolog-3 FL3-22 spectrometer at different voltages (using Keithley 2400 Sourcemeter). Time-resolved PL measurements were performed using a time-correlated single photon counting (TCSPC) system (PicoQuant PicoHarp 300) by exciting the colloidal samples with a NKT photonics femtosecond pulsed laser. PL spectra of different spots were obtained using a Princeton Instrument spectrometer excited with the same NKT laser.

***Morphological characterization*:** The morphology of the prepared perovskite crystals were characterized by bright field transmission electron microscopy (BF-TEM) (JEOL JEM-1011 with an 80kV accelerating voltage), high angle annular dark field scanning TEM (HAADF-STEM) (cubed FEI Titan microscope operating at 300 kV) and scanning electron microscopy (SEM) using a Gemini Ultra Plus at an electron accelerating voltage of 3 kV. X-ray diffraction (XRD) measurements were performed with a BRUKER D8 ADVANCE diffractometer using 8 keV Cu-K_α X-ray source. The theoretical cubic and orthorhombic phase $CsPbBr_3$ XRD patterns were taken from the crystallography open database (COD).

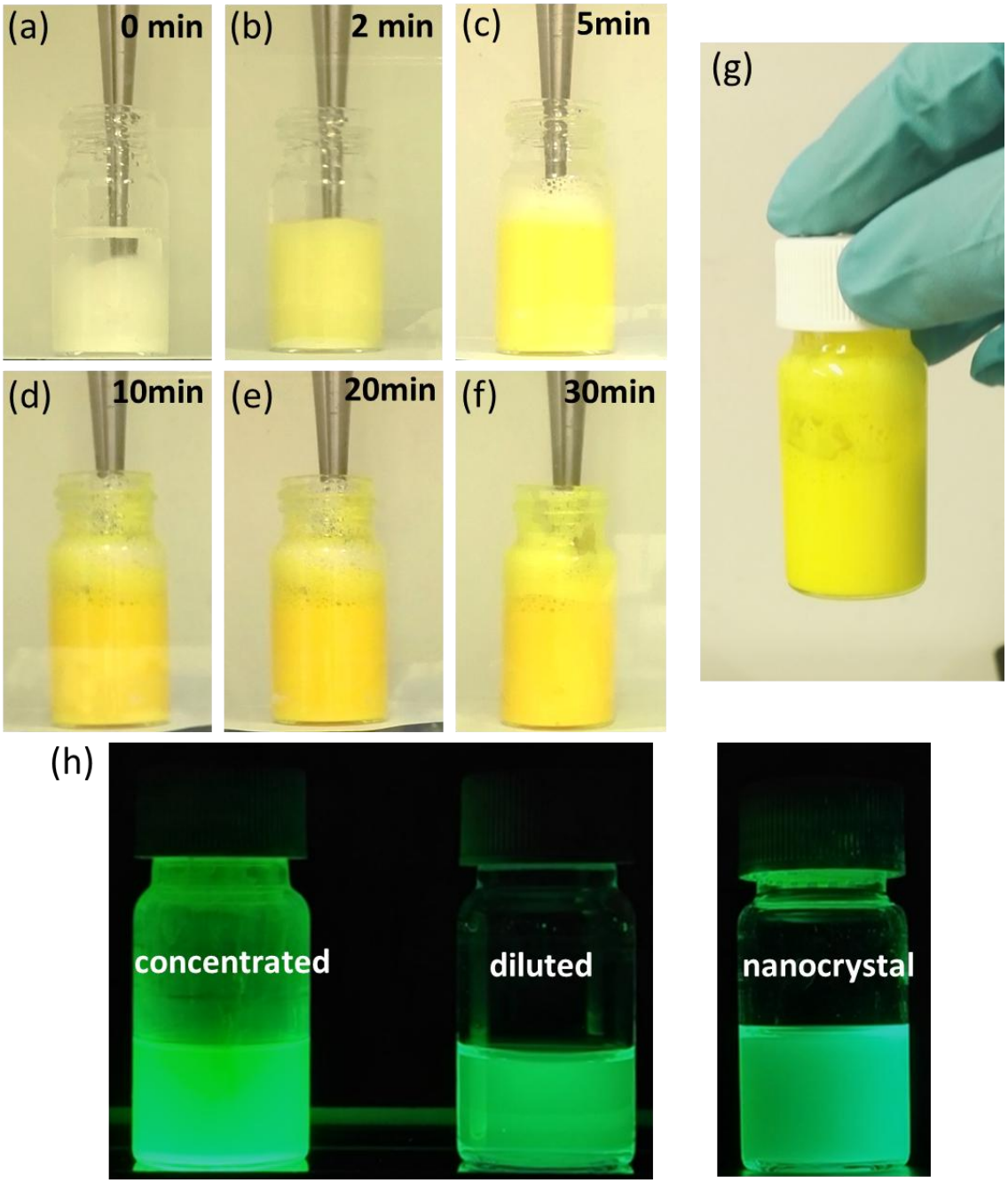

Figure **S1:** a-f) Photographs of the reaction medium recorded at different reaction times of SC synthesis. g) Photograph of the as-prepared SC colloidal dispersion after completion of the reaction. h) Photographs of the as-prepared, diluted SC and NC colloidal dispersion under UV-light (367 nm) illumination. One can see that concentrated SC colloidal solution exhibit pure green emission, whereas the diluted SC colloidal solutions shows cyan-green emission similar to the isolated NC colloidal dispersion.

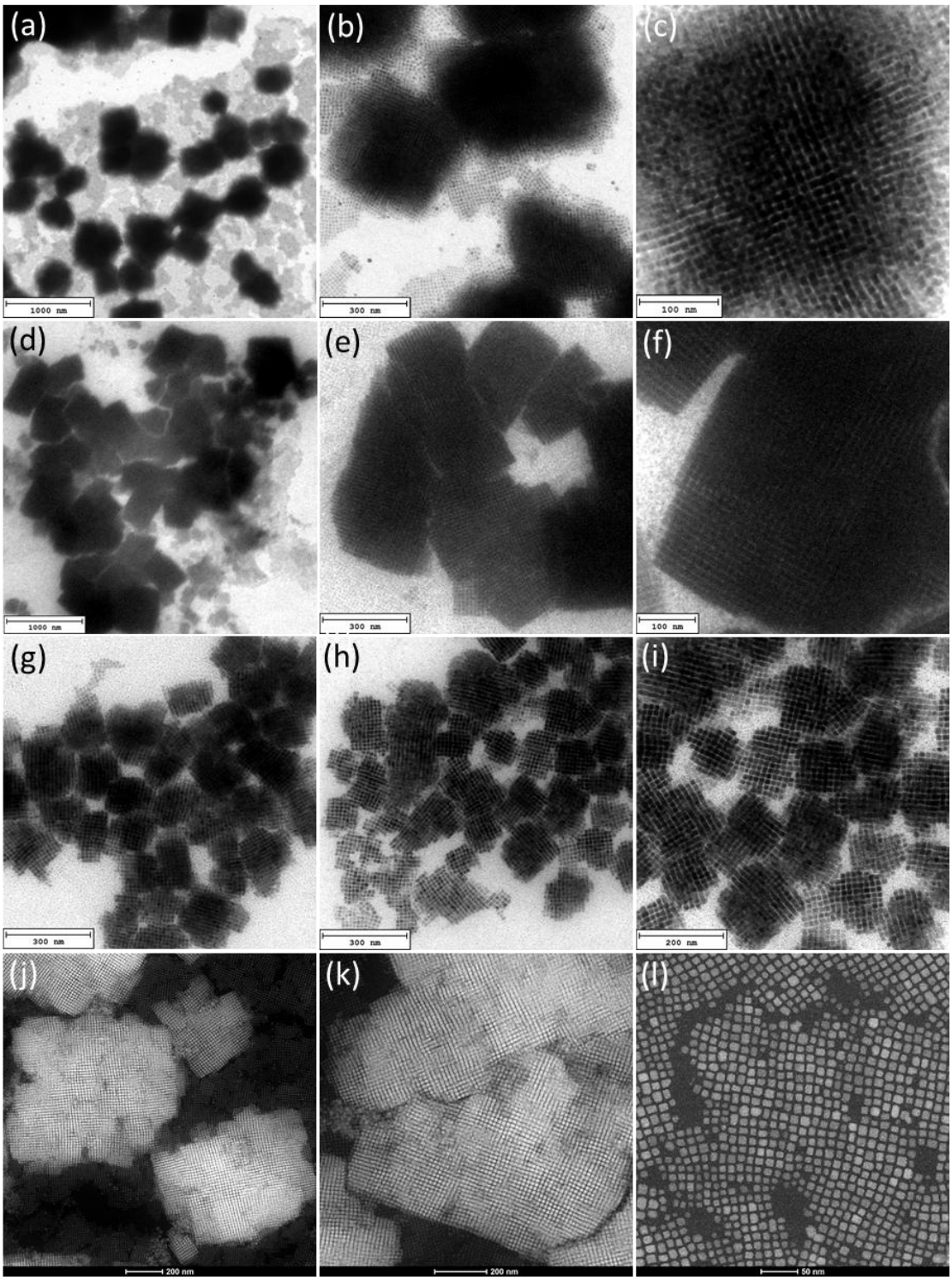

Figure **S2:** A broad overview of TEM (a-i) and HAADF-STEM (j & k) images of SCs in different magnifications. At low magnification, the SCs can be identified large polyhedral crystals with dark color, however the structure of superlattice can't be clearly seen in both TEM and HAADF-STEM. Once zoomed in, one can see that the SCs are actually made of nanocubes building blocks. (i) HAADF-STEM image of isolated $CsPbBr_3$ NCs obtained at low precursor concentration. The different between isolated NCs and SCs can be clearly seen in the images.

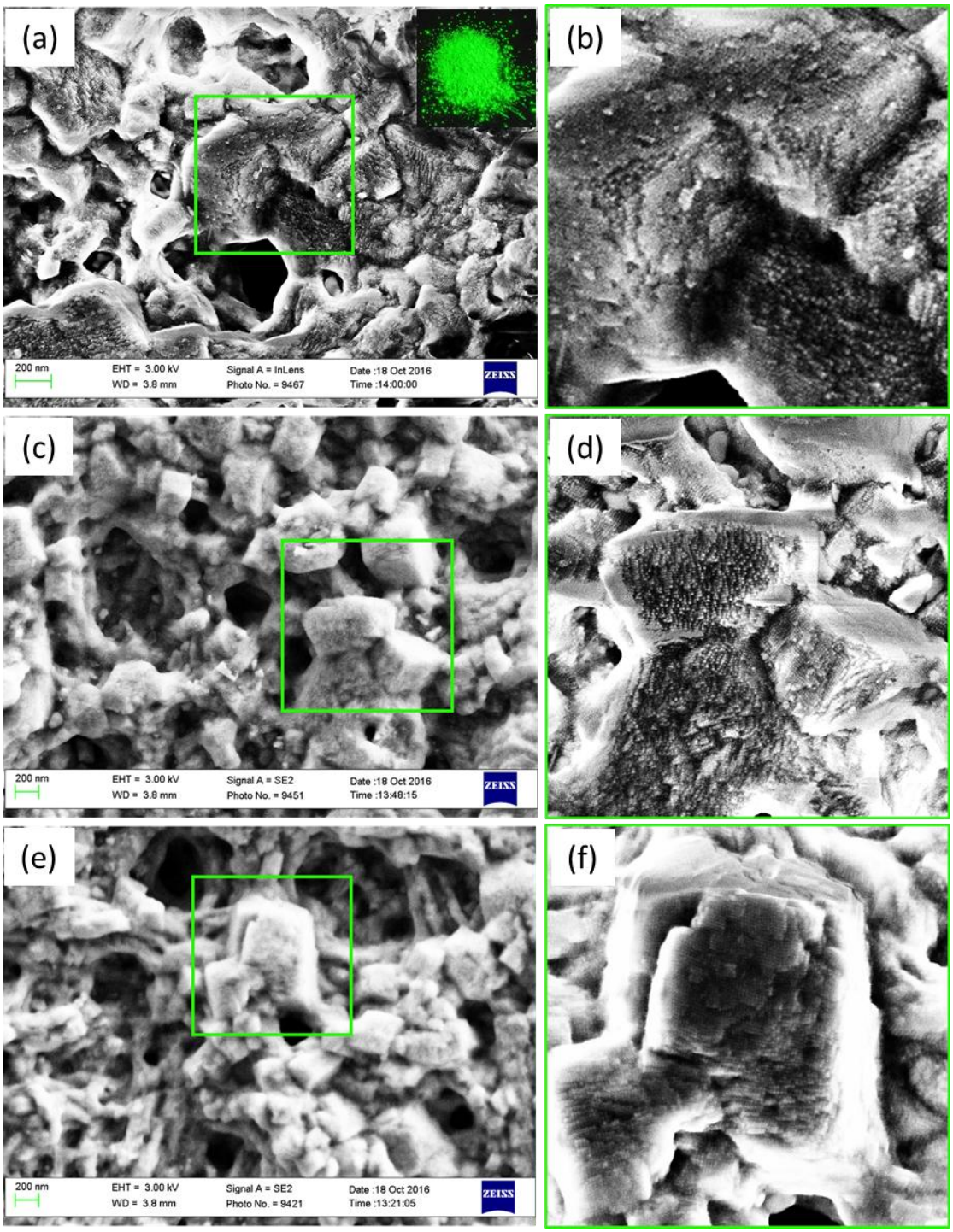

Figure **S3:** A broad overview of SEM images of SCs with different magnifications. The polyhedral shape of the supercrystals can be seen at low magnification (ac, c and e), while the images recorded at higher magnification shows that these polyhedral crystals are made of NC repeating units of size 10-15 nm.

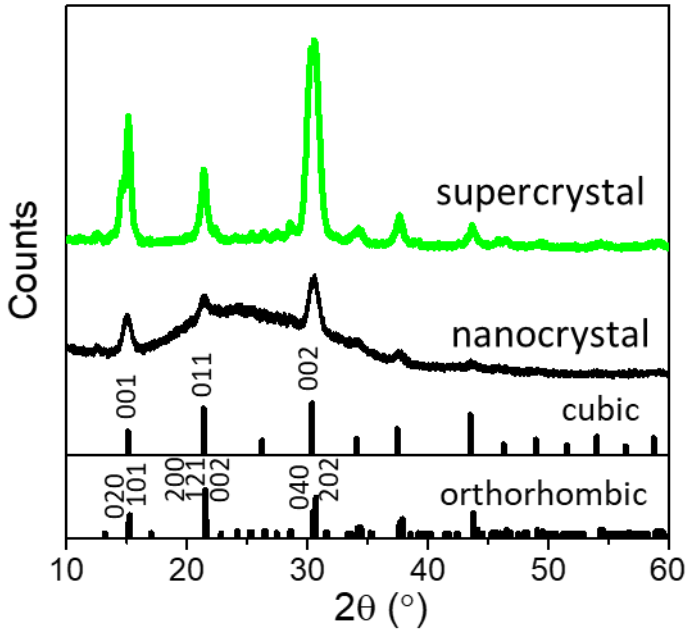

Figure **S4:** XRD data of SC film in comparison with nanocrystal. The patterns of cubic and orthorhombic phase CsPbBr3 perovskite are also shown as references. Both SC and NC show similar Bragg peak positions assigning to either orthorhombic or cubic phase. The supercrystals films show background free XRD peaks due to high density of the NCs in the films.

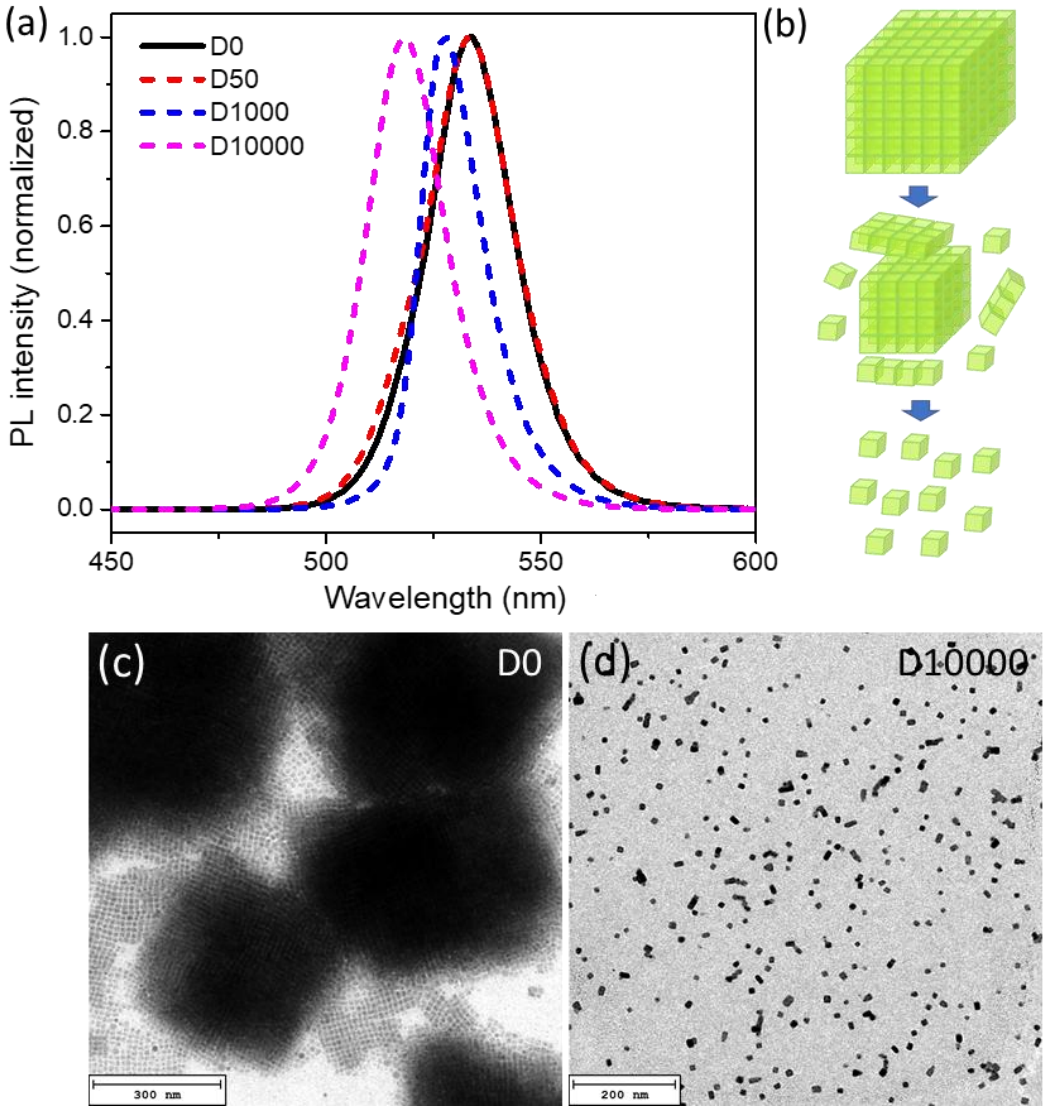

Figure **S5** (a) PL spectra of SC colloidal dispersions of different dilutions (0 to 10000). (b) Schematic illustration showing the disassembly of SCs into NCs by dilution. (c and d) corresponding TEM images of the colloids before and after dilution (D10000 times), respectively.

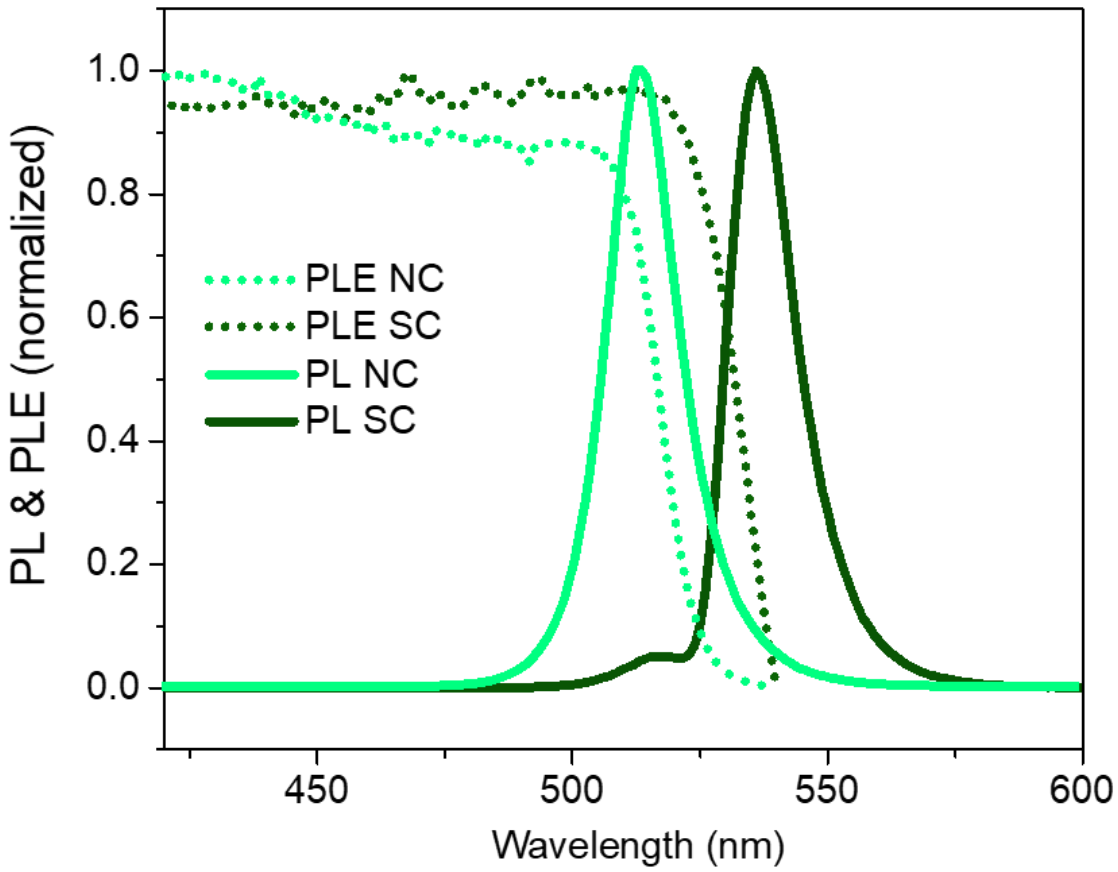

Figure **S6:** Photoluminescence excitation (PLE) (dotted lines) and PL spectra (solid lines) of NC (light green color) and SC (dark green color) films. It can be seen that the PLE of the SCs exhibit obvious redshift compared with that of the uncoupled NCs.

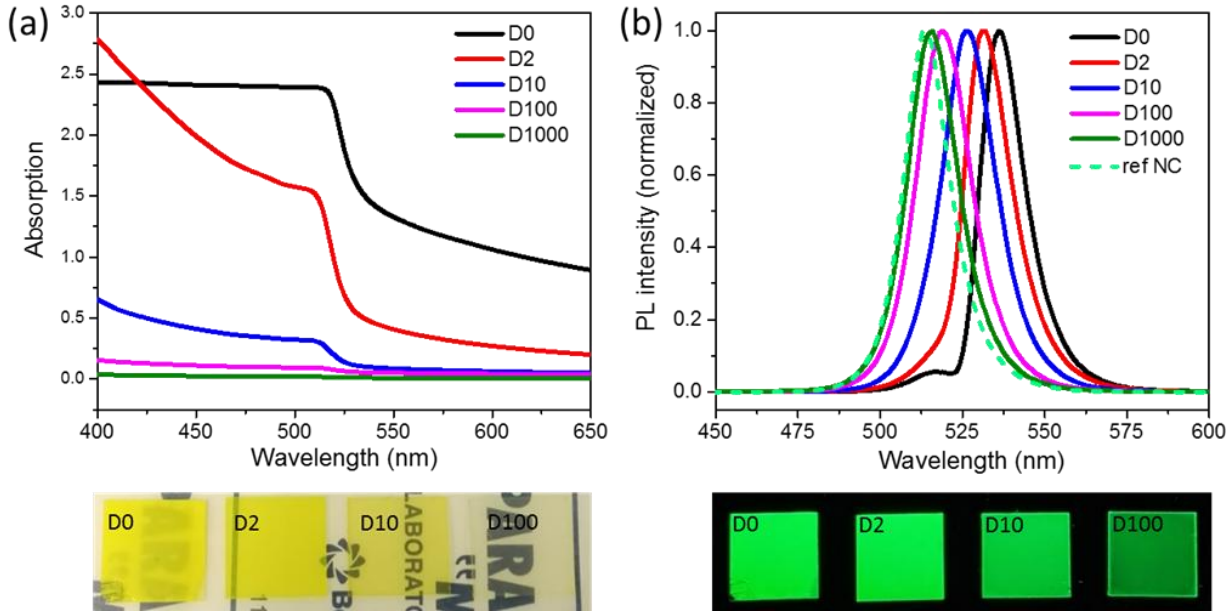

Figure **S7:** a) Absorption spectra of perovskite films prepared by spin-coating SC colloidal dispersion with varied dilutions (top) and the photograph of the films (bottom) recorded under room light. b) The corresponding PL spectra (top) and the photograph of the films (bottom) under UV light illumination. The PL spectra are normalized with respects of the perovskite film made of isolated NCs, which is also presented as a reference. Both the absorption onset and the PL peak position of the film show continuous blue shift with increasing dilution, and the PL spectra of the films made of diluted SCs (D1000) resembles that of isolated NC films, suggesting that the SCs disassemble into isolated NCs by dilution.

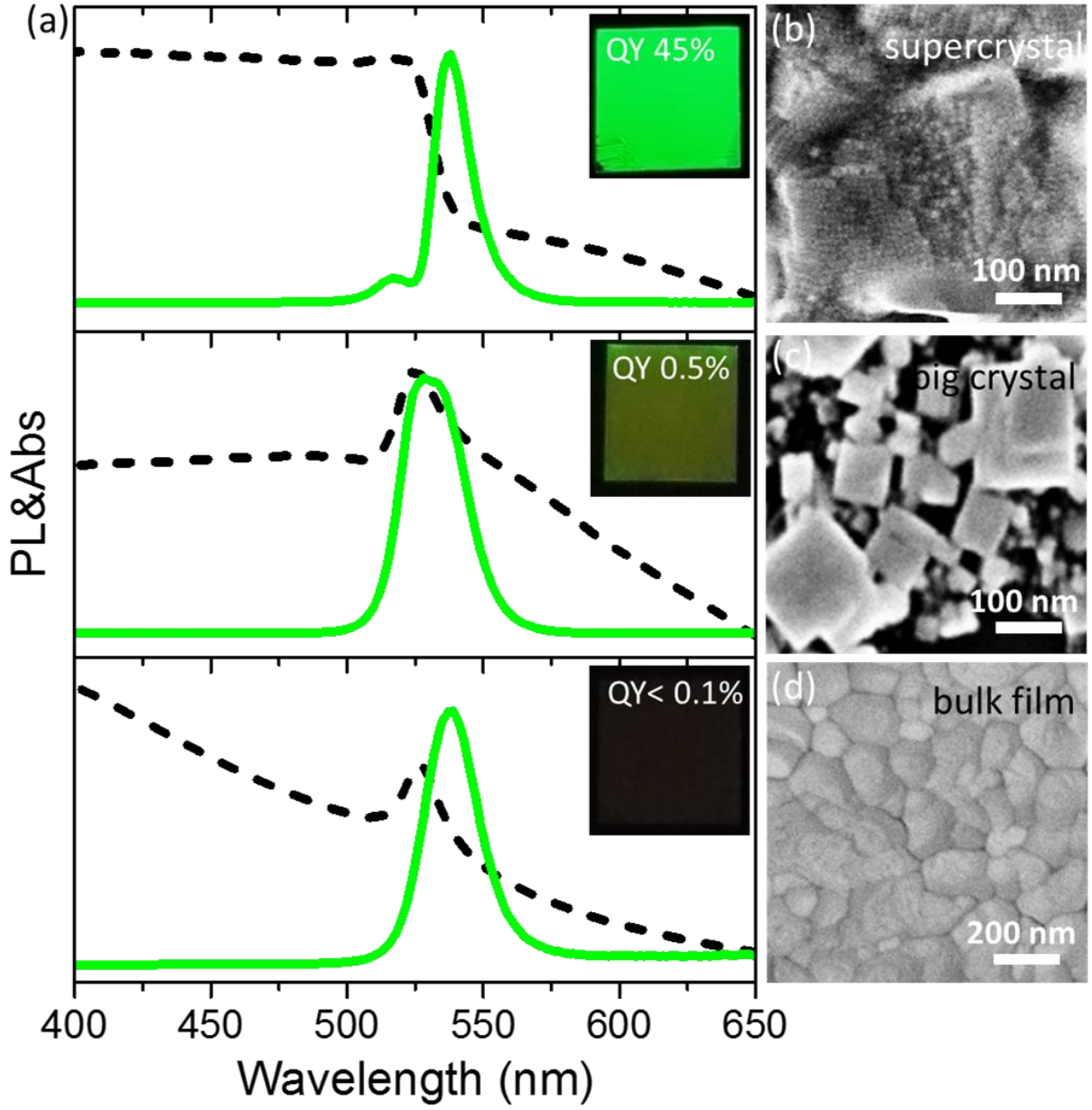

Figure **S8:** Comparison of morphology and optical properties between $CsPbBr_3$ perovskite made of SCs, bulk colloids and bulk films of. a) Absorption and PL spectra of SCs (top), large colloidal crystals (middle) and bulk film (down). The insets show the photographs of the films under UV (367 nm) light illumination and PL quantum yield of the each sample. (b-d) SEM images of the corresponding films shown in (a).

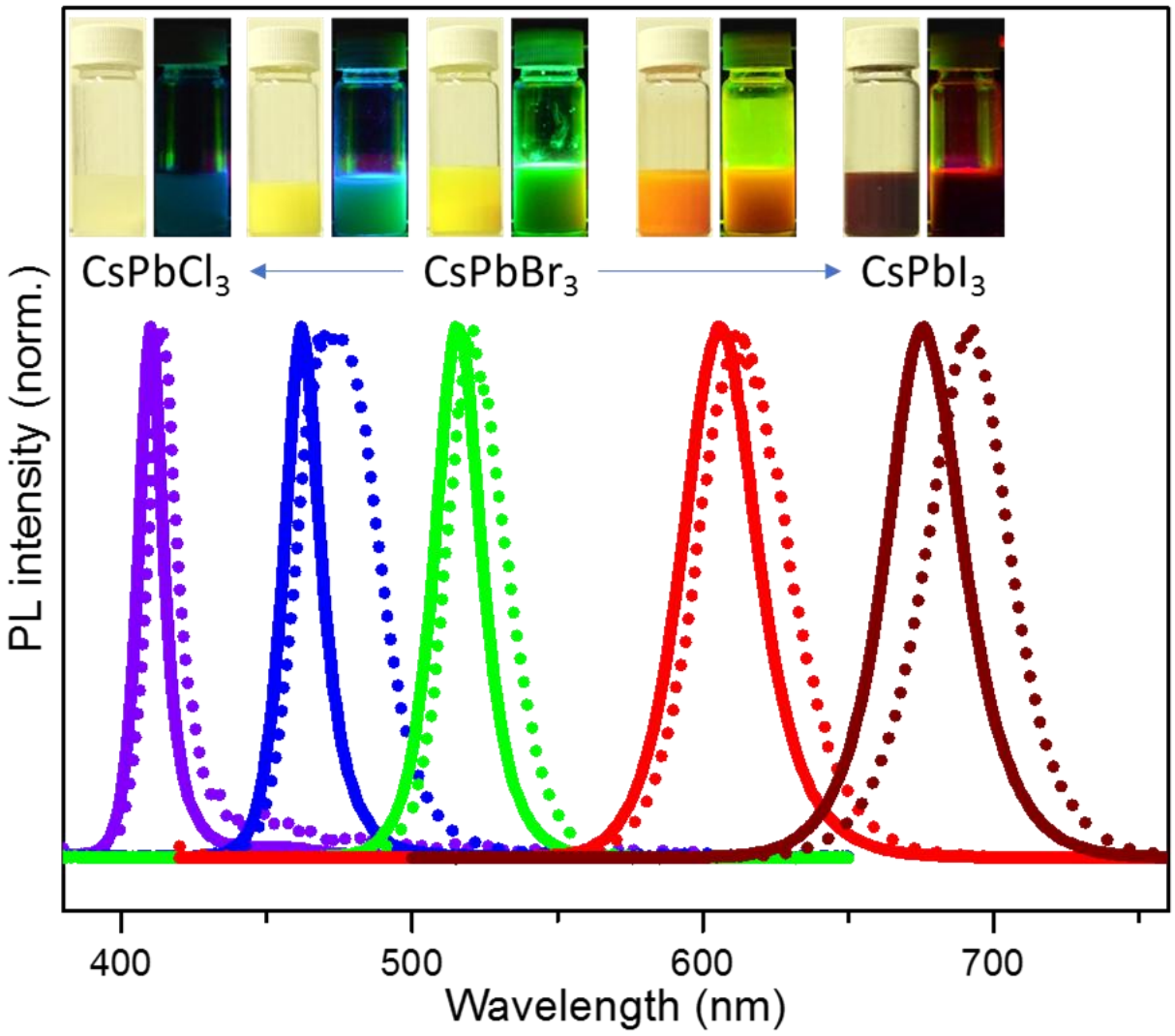

Figure **S9:** PL spectra of the concentrated (dotted lines) and diluted (solid lines) $CsPbX_3$ SC colloidal dispersions obtained by halide ion exchange on the $CsPbBr_3$ SC colloids. The photographs of the concentrated $CsPbX_3$ SC colloidal dispersions with different halide compositions under room light and UV illumination are shown in the inset.

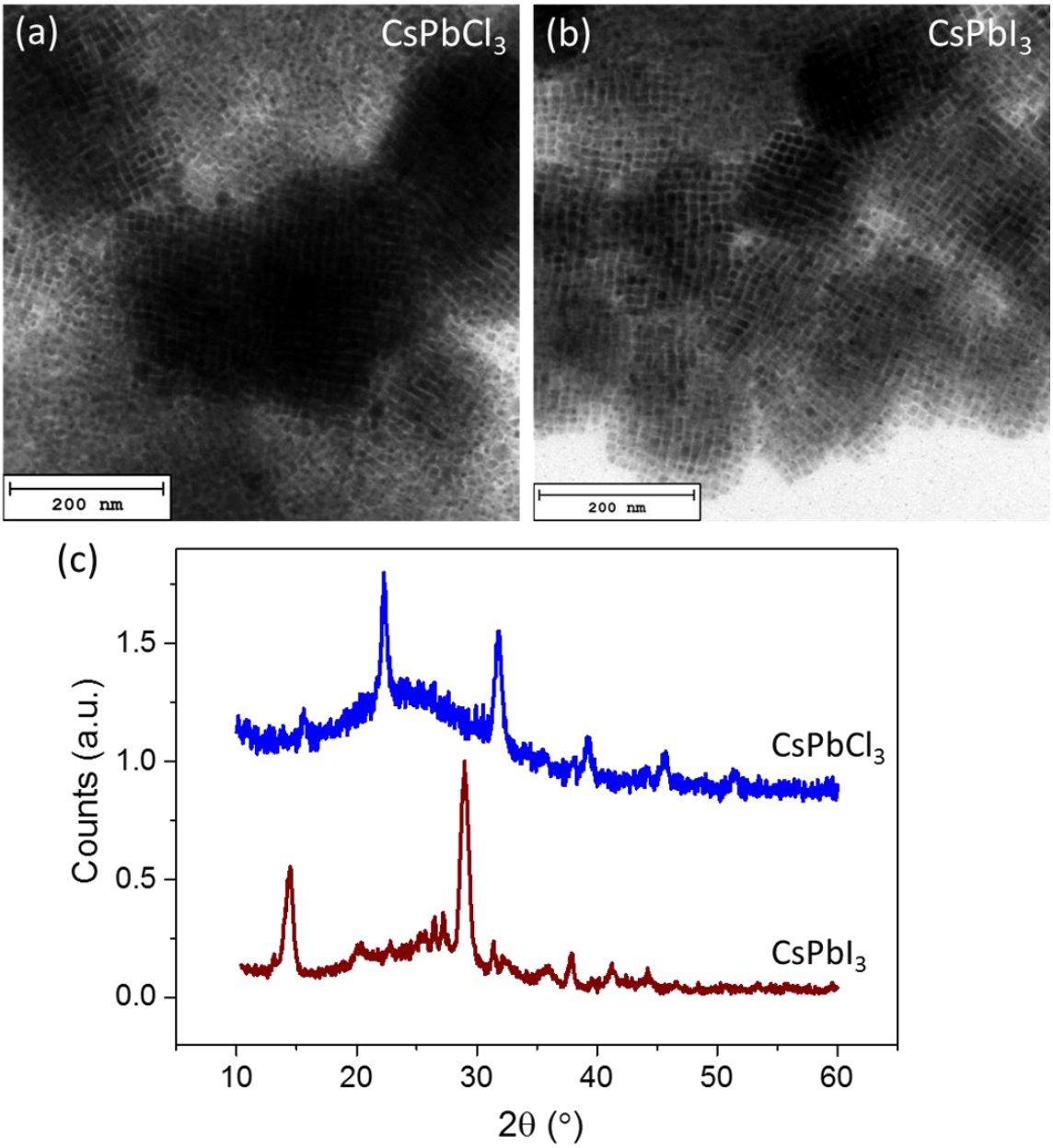

Figure **S10:** TEM images (a, b) and XRD patterns (c) of the $CsPbCl_3$ and $CsPbI_3$ SCs obtained by halide ion exchange on the as-synthesized colloidal $CsPbBr_3$ SCs. As shown by TEM images, assemblies can still be maintained after ion exchange. The XRD data demonstrate that the crystalline phase (orthorhombic or cubic) of the NCs in the assemblies remains unchanged after ion exchange.

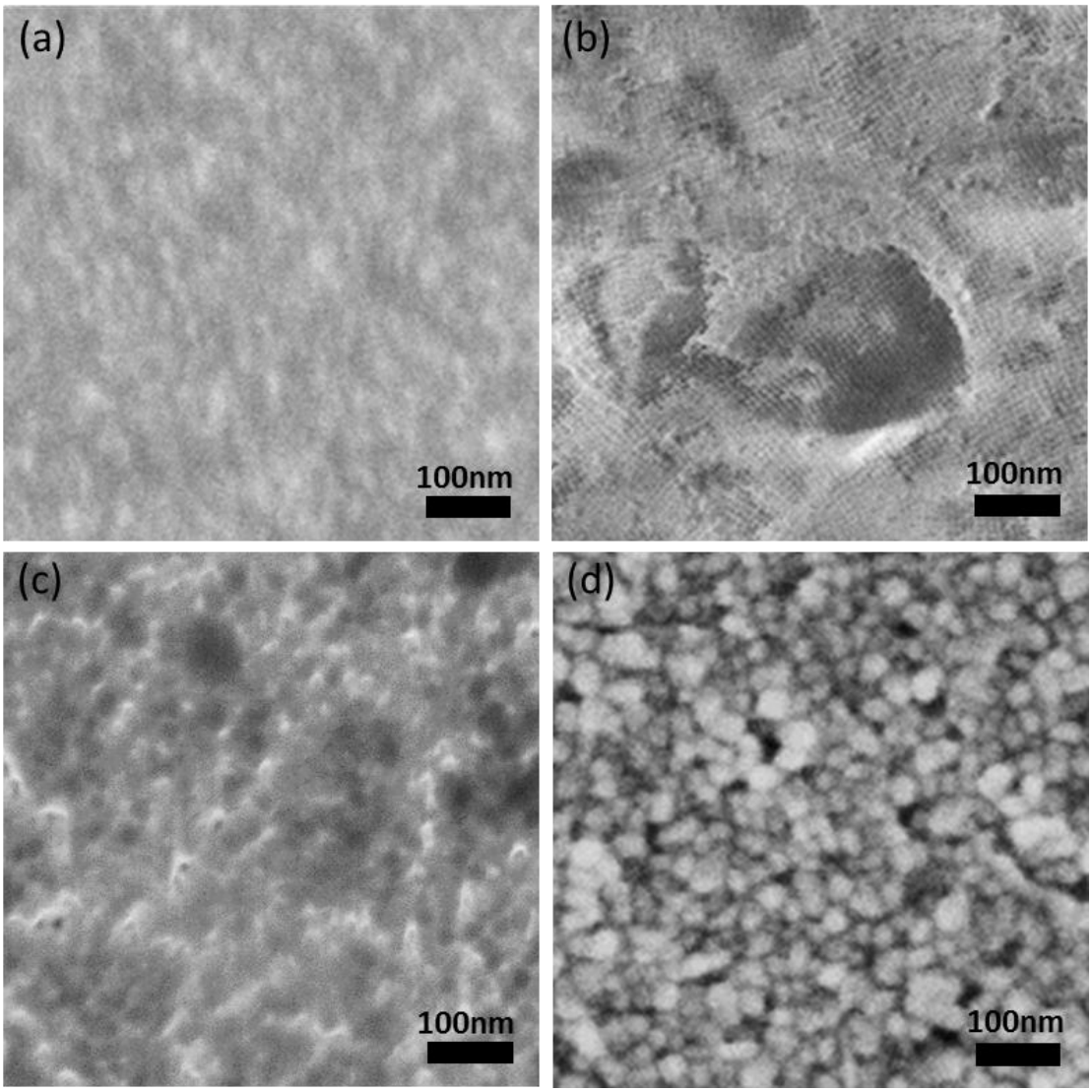

Figure **S11:** Top view SEM images of each functional layers in the solution-processed LED device. a) NiO_x b) perovskite c) PEI d) ZnO. It can be seen that each layer shows reasonable uniformity and pinhole free morphology. Especially, the perovskite film shows closely packed SCs exhibiting electronic coupling as aforementioned and manifests the pure green electroluminescence.

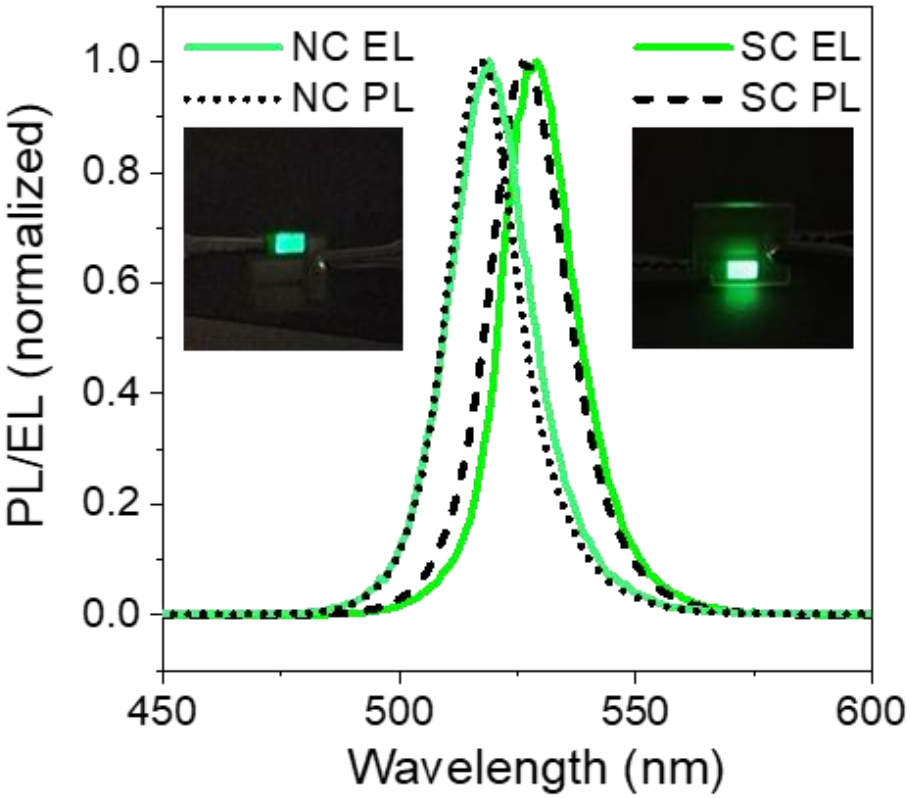

Figure **S12:** Comparison of the electroluminescence of LEDs fabricated using perovskite SCs and isolated NCs in the emitting layer. Both the NC and SC LEDs show strong, bright PL and EL. Insets show the photographs of the LEDs made of NCs and SCs.

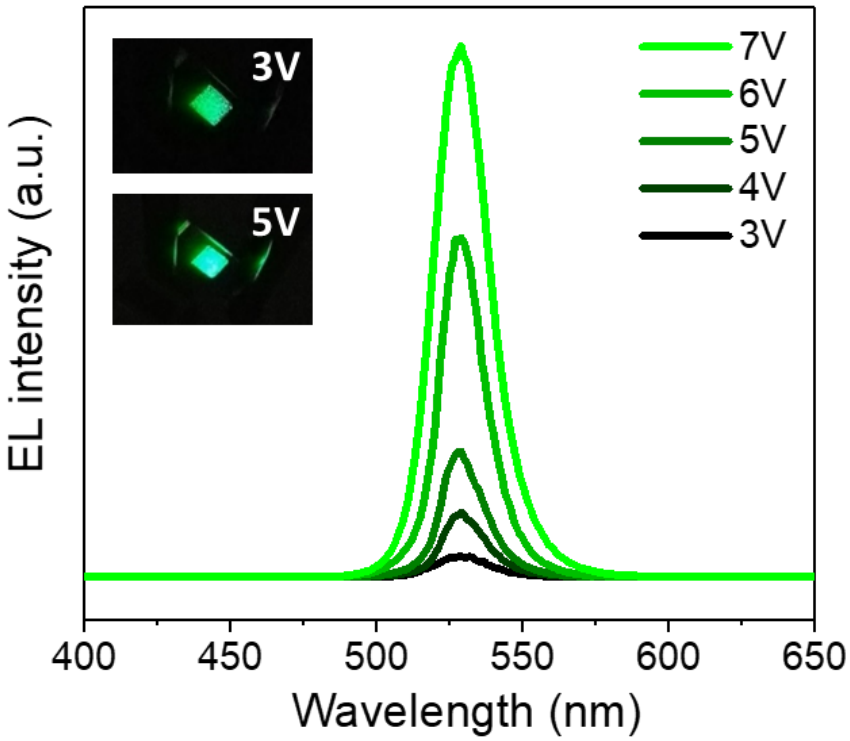

Figure **S13:** EL spectra of the solution-processed LED made of $CsPbBr_3$ SCs at different driving voltage. The EL intensity increased dramatically with the driving voltage while the peak position almost maintained the same at 530nm. Insets are the photos of the LED working at 3V (top) and 5V (bottom).

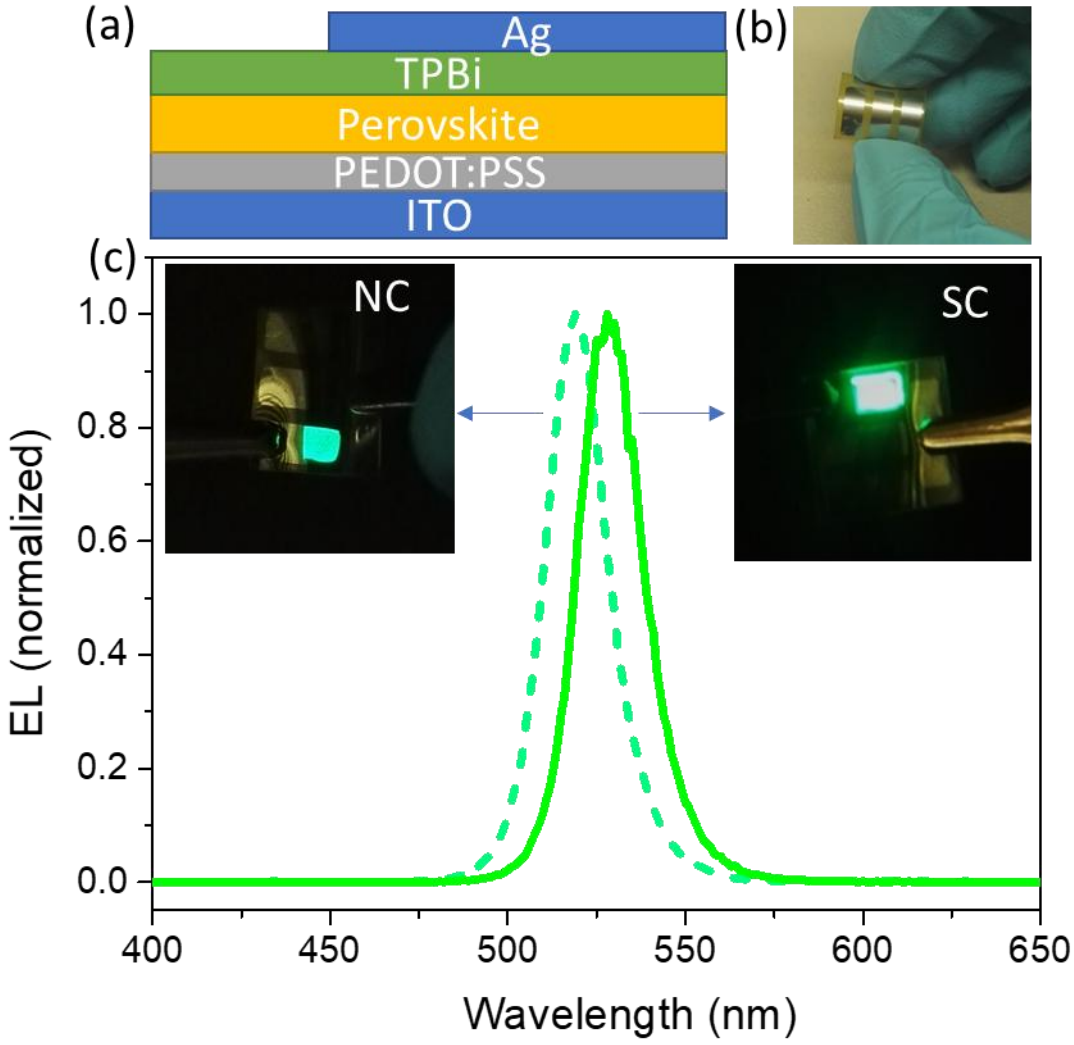

Figure **S14:** (a) Device architecture of flexible LED made out of $CsPbBr_3$ NCs or SCs. (b) Photograph of the fabricated flexible LED. (c) EL spectra of the flexible LEDs made out of $CsPbBr_3$ NCs (dashed line) or SCs (solid line). Photographs of the corresponding flexible LEDs working at a certain bending angle are shown in the insets.

[1] L. Protesescu, S. Yakunin, M. I. Bodnarchuk, F. Krieg, R. Caputo, C. H. Hendon, R. X. Yang, A. Walsh, M. V. Kovalenko, *Nano Lett.* **2015**, *15*, 3692.
[2] M. V. Kovalenko, L. Protesescu, M. I. Bodnarchuk, *Science* **2017**, *358*, 745.
[3] L. Dou, A. B. Wong, Y. Yu, M. Lai, N. Kornienko, S. W. Eaton, A. Fu, C. G. Bischak, J. Ma, T. Ding, N. S. Ginsberg, L.-W. Wang, A. P. Alivisatos, P. Yang, *Science* **2015**, *349*, 1518.
[4] S. D. Stranks, G. E. Eperon, G. Grancini, C. Menelaou, M. J. P. Alcocer, T. Leijtens, L. M. Herz, A. Petrozza, H. J. Snaith, *Science* **2013**, *342*, 341.
[5] G. Xing, N. Mathews, S. Sun, S. S. Lim, Y. M. Lam, M. Grätzel, S. Mhaisalkar, T. C. Sum, *Science* **2013**, *342*, 344.
[6] Q. A. Akkerman, M. Gandini, F. Di Stasio, P. Rastogi, F. Palazon, G. Bertoni, J. M. Ball, M. Prato, A. Petrozza, L. Manna, *Nat. Energy* **2016**, *2*, 16194.

[7] Y. Zhang, J. Liu, Z. Wang, Y. Xue, Q. Ou, L. Polavarapu, J. Zheng, X. Qi, Q. Bao, *Chem. Commun.* **2016**, *52*, 13637.
[8] H. Huang, L. Polavarapu, J. A. Sichert, A. S. Susha, A. S. Urban, A. L. Rogach, *NPG Asia Mater.* **2016**, *8*, e328.
[9] Y. Wang, X. Li, J. Song, L. Xiao, H. Zeng, H. Sun, *Adv. Mater.* **2015**, *27*, 7101.
[10] L. Polavarapu, B. Nickel, J. Feldmann, A. S. Urban, *Advanced Energy Materials* **2017**, *7*, n/a.
[11] X. Li, Y. Wang, H. Sun, H. Zeng, *Adv. Mater.* **2017**, *29*.
[12] L. C. Schmidt, A. Pertegas, S. Gonzalez-Carrero, O. Malinkiewicz, S. Agouram, G. M. Espallargas, H. J. Bolink, R. E. Galian, J. Perez-Prieto, *J. Am. Chem. Soc.* **2014**, *136*, 850.
[13] A. Swarnkar, V. K. Ravi, A. Nag, *ACS Energy Lett.* **2017**, *2*, 1089.
[14] A. Swarnkar, R. Chulliyil, V. K. Ravi, M. Irfanullah, A. Chowdhury, A. Nag, *Angew. Chem. Int. Ed.* **2015**, *54*, 15424.
[15] J. Liu, Y. Xue, Z. Wang, Z.-Q. Xu, C. Zheng, B. Weber, J. Song, Y. Wang, Y. Lu, Y. Zhang, Q. Bao, *ACS Nano* **2016**, *10*, 3536.
[16] F. Zhang, H. Zhong, C. Chen, X.-g. Wu, X. Hu, H. Huang, J. Han, B. Zou, Y. Dong, *ACS Nano* **2015**, *9*, 4533.
[17] H. Huang, F. Zhao, L. Liu, F. Zhang, X.-g. Wu, L. Shi, B. Zou, Q. Pei, H. Zhong, *ACS Appl. Mater. Interfaces* **2015**, *7*, 28128.
[18] M. C. Weidman, M. Seitz, S. D. Stranks, W. A. Tisdale, *ACS Nano* **2016**, *10*, 7830.
[19] X. Zhang, H. Lin, H. Huang, C. Reckmeier, Y. Zhang, W. C. H. Choy, A. L. Rogach, *Nano Lett.* **2016**, *16*, 1415.
[20] M. Chen, Y. T. Zou, L. Z. Wu, Q. Pan, D. Yang, H. C. Hu, Y. S. Tan, Q. X. Zhong, Y. Xu, H. Y. Liu, B. Q. Sun, Q. Zhang, *Adv. Funct. Mater.* **2017**, *27*.
[21] Y. Bekenstein, B. A. Koscher, S. W. Eaton, P. D. Yang, A. P. Alivisatos, *J. Am. Chem. Soc.* **2015**, *137*, 16008.
[22] G. Nedelcu, L. Protesescu, S. Yakunin, M. I. Bodnarchuk, M. J. Grotevent, M. V. Kovalenko, *Nano Lett.* **2015**, *15*, 5635.
[23] Q. A. Akkerman, V. D'Innocenzo, S. Accornero, A. Scarpellini, A. Petrozza, M. Prato, L. Manna, *J. Am. Chem. Soc.* **2015**, *137*, 10276.
[24] Y. Tong, E. Bladt, M. F. Aygüler, A. Manzi, K. Z. Milowska, V. A. Hintermayr, P. Docampo, S. Bals, A. S. Urban, L. Polavarapu, J. Feldmann, *Angew. Chem. Int. Ed.* **2016**, *55*, 13887.
[25] J. A. Sichert, Y. Tong, N. Mutz, M. Vollmer, S. Fischer, K. Z. Milowska, R. García Cortadella, B. Nickel, C. Cardenas-Daw, J. K. Stolarczyk, A. S. Urban, J. Feldmann, *Nano Lett.* **2015**, *15*, 6521.
[26] V. A. Hintermayr, A. F. Richter, F. Ehrat, M. Döblinger, W. Vanderlinden, J. A. Sichert, Y. Tong, L. Polavarapu, J. Feldmann, A. S. Urban, *Adv. Mater.* **2016**, *28*, 9478.
[27] Y. Tong, F. Ehrat, W. Vanderlinden, C. Cardenas-Daw, J. K. Stolarczyk, L. Polavarapu, A. S. Urban, *ACS Nano* **2016**, *10*, 10936.
[28] Q. A. Akkerman, S. G. Motti, A. R. Srimath Kandada, E. Mosconi, V. D'Innocenzo, G. Bertoni, S. Marras, B. A. Kamino, L. Miranda, F. De Angelis, A. Petrozza, M. Prato, L. Manna, *J. Am. Chem. Soc.* **2016**, *138*, 1010.
[29] Y. Bekenstein, B. A. Koscher, S. W. Eaton, P. Yang, A. P. Alivisatos, *J. Am. Chem. Soc.* **2015**, *137*, 16008.
[30] D. Zhang, S. W. Eaton, Y. Yu, L. Dou, P. Yang, *J. Am. Chem. Soc.* **2015**, *137*, 9230.
[31] Y. Tong, B. J. Bohn, E. Bladt, K. Wang, P. Müller-Buschbaum, S. Bals, A. S. Urban, L. Polavarapu, J. Feldmann, *Angew. Chem. Int. Ed.* **2017**, *56*, 13887.
[32] H. Huang, B. Chen, Z. Wang, T. F. Hung, A. S. Susha, H. Zhong, A. L. Rogach, *Chemical Science* **2016**, *7*, 5699.

[33] S. Pathak, N. Sakai, F. Wisnivesky Rocca Rivarola, S. D. Stranks, J. Liu, G. E. Eperon, C. Ducati, K. Wojciechowski, J. T. Griffiths, A. A. Haghighirad, A. Pellaroque, R. H. Friend, H. J. Snaith, *Chem. Mater.* **2015**, *27*, 8066.
[34] F. Nippert, S. Y. Karpov, G. Callsen, B. Galler, T. Kure, C. Nenstiel, M. R. Wagner, M. Straßburg, H.-J. Lugauer, A. Hoffmann, *Appl. Phys. Lett.* **2016**, *109*.
[35] I. Lignos, L. Protesescu, D. B. Emiroglu, R. Maceiczyk, S. Schneider, M. V. Kovalenko, A. J. deMello, *Nano Lett.* **2018**, 10.1021/acs.nanolett.7b04838.
[36] T. Sugaya, T. Amano, M. Mori, S. Niki, *Appl. Phys. Lett.* **2010**, *97*, 043112.
[37] M. Scheibner, T. Schmidt, L. Worschech, A. Forchel, G. Bacher, T. Passow, D. Hommel, *Nat. Phys.* **2007**, *3*, 106.
[38] Y. Rakita, N. Kedem, S. Gupta, A. Sadhanala, V. Kalchenko, M. L. Böhm, M. Kulbak, R. H. Friend, D. Cahen, G. Hodes, *Cryst. Growth Des.* **2016**, *16*, 5717.
[39] J. Zhang, A. A. Lutich, A. S. Susha, M. Döblinger, C. Mauser, A. O. Govorov, A. L. Rogach, F. Jäckel, J. Feldmann, *Journal of Applied Physics* **2010**, *107*, 123516.
[40] Z. Nie, A. Petukhova, E. Kumacheva, *Nat. Nanotech.* **2009**, *5*, 15.
[41] C. R. Kagan, C. B. Murray, *Nat. Nanotech.* **2015**, *10*, 1013.
[42] M. P. Pileni, *J. Phys. Chem. B* **2001**, *105*, 3358.
[43] Y. Min, M. Akbulut, K. Kristiansen, Y. Golan, J. Israelachvili, *Nat. Mater.* **2008**, *7*, 527.
[44] L. Motte, F. Billoudet, E. Lacaze, M.-P. Pileni, *Adv. Mater.* **1996**, *8*, 1018.
[45] M. Grzelczak, J. Vermant, E. M. Furst, L. M. Liz-Marzán, *ACS Nano* **2010**, *4*, 3591.
[46] N. Soetan, W. R. Erwin, A. M. Tonigan, D. G. Walker, R. Bardhan, *J. Phys. Chem. C* **2017**, *121*, 18186.
[47] Z. Dang, J. Shamsi, F. Palazon, M. Imran, Q. A. Akkerman, S. Park, G. Bertoni, M. Prato, R. Brescia, L. Manna, *ACS Nano* **2017**, *11*, 2124.
[48] L.-X. Dai, X.-Y. Wang, X.-Y. Zheng, Y.-W. Zhang, *Chem. Commun.* **2016**, *52*, 5023.
[49] C.-W. Yang, C.-Y. Chiu, M. H. Huang, *Chem. Mater.* **2014**, *26*, 4882.
[50] L. Protesescu, S. Yakunin, M. I. Bodnarchuk, F. Krieg, R. Caputo, C. H. Hendon, R. X. Yang, A. Walsh, M. V. Kovalenko, *Nano Lett.* **2015**, *15*, 3692.
[51] D. N. Dirin, I. Cherniukh, S. Yakunin, Y. Shynkarenko, M. V. Kovalenko, *Chem. Mater.* **2016**, *28*, 8470.
[52] Y. Li, Z.-F. Shi, S. Li, L.-Z. Lei, H.-F. Ji, D. Wu, T.-T. Xu, Y.-T. Tian, X.-J. Li, *Journal of Materials Chemistry C* **2017**, *5*, 8355.
[53] D. V. Talapin, J.-S. Lee, M. V. Kovalenko, E. V. Shevchenko, *Chem. Rev.* **2010**, *110*, 389.
[54] J. Even, L. Pedesseau, C. Katan, *ChemPhysChem* **2014**, *15*, 3733.
[55] L. M. Pazos-Outón, M. Szumilo, R. Lamboll, J. M. Richter, M. Crespo-Quesada, M. Abdi-Jalebi, H. J. Beeson, M. Vrućinić, M. Alsari, H. J. Snaith, B. Ehrler, R. H. Friend, F. Deschler, *Science* **2016**, *351*, 1430.
[56] J. Song, J. Li, X. Li, L. Xu, Y. Dong, H. Zeng, *Advanced Materials* **2015**, *27*, 7162.
[57] L. Protesescu, S. Yakunin, M. I. Bodnarchuk, F. Bertolotti, N. Masciocchi, A. Guagliardi, M. V. Kovalenko, *J Am Chem Soc* **2016**, *138*, 14202.
[58] G. Li, F. W. R. Rivarola, N. J. L. K. Davis, S. Bai, T. C. Jellicoe, F. de la Peña, S. Hou, C. Ducati, F. Gao, R. H. Friend, N. C. Greenham, Z.-K. Tan, *Advanced Materials* **2016**, *28*, 3528.
[59] S. Woo, W. Hyun Kim, H. Kim, Y. Yi, H.-K. Lyu, Y. Kim, *Advanced Energy Materials* **2014**, *4*, n/a.
[60] S. Kumar, J. Jagielski, N. Kallikounis, Y.-H. Kim, C. Wolf, F. Jenny, T. Tian, C. J. Hofer, Y.-C. Chiu, W. J. Stark, T.-W. Lee, C.-J. Shih, *Nano Lett.* **2017**, *17*, 5277.

[61] Y. Tong, E. Bladt, M. F. Aygüler, A. Manzi, K. Z. Milowska, V. A. Hintermayr, P. Docampo, S. Bals, A. S. Urban, L. Polavarapu, J. Feldmann, *Angew. Chem. Int. Ed.* **2016**, *55*, 13887.
[62] J. B. Hoffman, G. Zaiats, I. Wappes, P. V. Kamat, *Chemistry of Materials* **2017**, *29*, 9767.
[63] E.-P. Yao, Z. Yang, L. Meng, P. Sun, S. Dong, Y. Yang, Y. Yang, *Advanced Materials* **2017**, *29*, n/a.